

A neural basis for tonic suppression of sodium appetite

Seahyung Park¹, Kevin W. Williams², Chen Liu^{2,3*} and Jong-Woo Sohn^{1*}

Sodium appetite is a powerful form of motivation that can drive ingestion of high, yet aversive concentrations of sodium in animals that are depleted of sodium. However, in normal conditions, sodium appetite is suppressed to prevent homeostatic deviations. Although molecular and neural mechanisms underlying the stimulation of sodium appetite have received much attention recently, mechanisms that inhibit sodium appetite remain largely obscure. Here we report that serotonin 2c receptor (Htr2c)-expressing neurons in the lateral parabrachial nucleus (LPBN^{Htr2c} neurons) inhibit sodium appetite. Activity of these neurons is regulated by bodily sodium content, and their activation can rapidly suppress sodium intake. Conversely, inhibition of these neurons specifically drives sodium appetite, even during euvoletic conditions. Notably, the physiological role of Htr2c expressed by LPBN neurons is to disinhibit sodium appetite. Our results suggest that LPBN^{Htr2c} neurons act as a brake against sodium appetite and that their alleviation is required for the full manifestation of sodium appetite.

Sodium ion (Na⁺) is an essential mineral to maintain extracellular fluid (ECF) and blood volume. Depletion of sodium leads to an increase in sodium appetite—a strong motivation for animals to consume otherwise aversive concentrations of sodium¹. Recently, several studies identified neural circuits and molecular mechanisms underlying the promotion of sodium appetite^{2–4}. However, sodium appetite is not strongly manifested in normal conditions, suggesting that it might be suppressed. Indeed, high concentrations of sodium are typically aversive in the euvoletic state, which is in part mediated by a peripheral mechanism⁵. However, a central mechanism underlying the suppression of sodium appetite is currently unknown. Previous pharmacological studies suggested that the LPBN plays a role in suppressing sodium appetite^{6,7}. However, lesions to the LPBN failed to increase sodium appetite^{8,9}, which otherwise seems to suggest that the LPBN is not involved in suppressing sodium appetite during euvoletic states. This discrepancy might be due in part to the heterogeneous nature of the LPBN, as this nucleus has been shown to also contain a population of neurons that putatively promote sodium appetite¹⁰. Thus, the identity of LPBN neuronal subpopulations that suppress sodium appetite remains to be revealed.

Brain serotonin receptors were proposed to control sodium appetite, but the results were not consistent between studies, possibly owing to the use of different drugs^{11,12}. Likewise, infusions of drugs that affect serotonergic signaling within the LPBN have been shown to have mixed effects on sodium intake^{13,14}. These pharmacological studies suggest that serotonergic mechanisms within the LPBN contribute to alter sodium appetite. However, they lack cellular and temporal specificity, which limits the interpretation of these results. Notably, no information is currently available regarding the physiological role of specific types of serotonin receptors expressed by LPBN neurons in regulating sodium balance.

To resolve the issues raised by past studies, we genetically segregated a population of LPBN neurons that express Htr2c and investigated their potential role and the relevant circuitry in mediating the suppression of sodium appetite. Furthermore, we explored the

physiological role of this neuronal population in the control of sodium appetite.

Results

LPBN^{Htr2c} neurons are regulated by bodily sodium content. To examine whether LPBN^{Htr2c} neurons respond to high concentrations of sodium, we performed fluorescence in situ hybridization for *Fos*. Mice were gastrically loaded via oral gavage with either saline (154 mM NaCl) or hypertonic saline (1.5 M NaCl) and then killed 25 min later. Consistent with previous reports^{15,16}, we saw a robust increase in *Fos* expression throughout the LPBN (Extended Data Fig. 1). In particular, we found an increase of *Fos* in *Htr2c*-expressing neurons (Fig. 1a–c), suggesting that LPBN^{Htr2c} neurons are capable of responding to high concentrations of sodium. We also measured *Fos* within neurons that expressed serotonin 1B receptor (*Htr1b*) or forkhead box protein 2 (*Foxp2*) in the LPBN, which were implicated in the regulation of sodium balance. *Htr1b* is another major serotonergic receptor in the LPBN, but we found little difference in *Fos* expression in *Htr1b*-expressing neurons (Fig. 1c,d). We also observed little change in *Fos* in *Foxp2*-expressing neurons (Fig. 1c,e), consistent with a previous report showing that *Foxp2* neurons in the LPBN were instead responsive to sodium depletion¹⁰. We next examined co-localization between transcripts of *Htr2c* and other genes that are expressed in the LPBN. We found little co-localization between *Htr2c* and *Htr1b* transcripts (2.1% ± 0.5%) (Fig. 1f,g) and a small amount of co-localization between *Htr2c* and *Foxp2* transcripts (10.7% ± 1.9%) (Fig. 1f,h). Because oxytocin receptor (*Oxtr*)-expressing LPBN neurons were reported to regulate fluid intake¹⁷, we measured their co-localization with *Htr2c* transcripts and found that 2.5% ± 0.3% of LPBN^{Htr2c} neurons co-express *Oxtr* (Fig. 1f,i). Together, these results suggest that LPBN^{Htr2c} neurons are largely distinct from *Htr1b* neurons, sodium appetite-promoting *Foxp2* neurons and fluid-intake-regulating *Oxtr* neurons.

Because hypertonic saline might cause general visceral aversion as well as a sodium-aversive state, thus complicating the interpretation of these results, we sought to investigate whether

¹Department of Biological Sciences, Korea Advanced Institute of Science and Technology, Daejeon, Korea. ²The Center for Hypothalamic Research, Department of Internal Medicine, University of Texas Southwestern Medical Center, Dallas, TX, USA. ³Department of Neuroscience, University of Texas Southwestern Medical Center, Dallas, TX, USA. *e-mail: chen.liu@utsouthwestern.edu; jwsohn@kaist.ac.kr

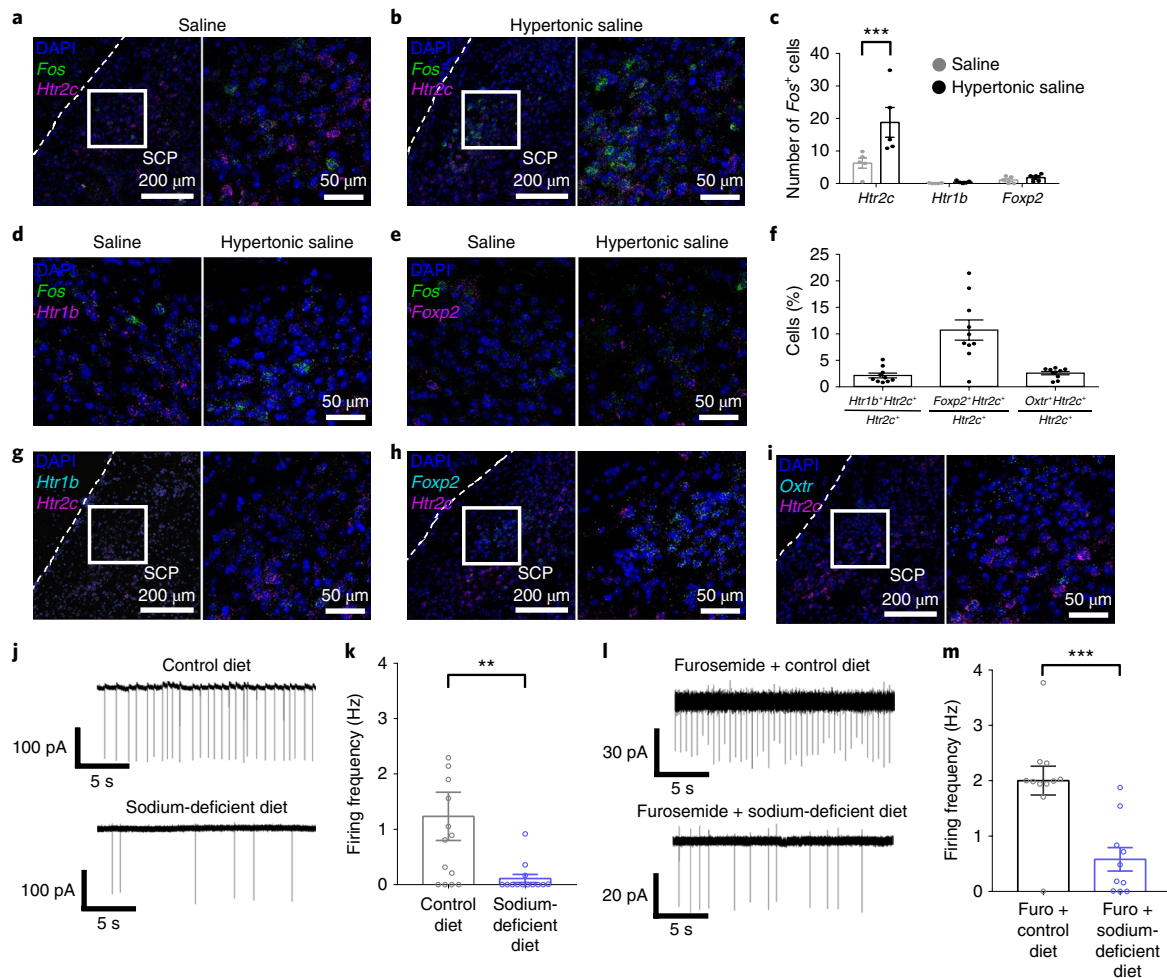


Fig. 1 | LPBN^{Htr2c} neurons are regulated by bodily sodium content. **a**, Co-localization of *Fos* and *Htr2c* transcripts in the LPBN after gastric loading of saline. Left: low magnification picture; right: higher magnification of the area inside the white box. Scale bars, 200 μm (left) and 50 μm (right). Dashed lines indicate ventral spinocerebellar tract. SCP, superior cerebellar peduncle. **b**, Co-localization of *Fos* and *Htr2c* transcripts in the LPBN after gastric loading of hypertonic saline. Left: low magnification picture; right: higher magnification of the area inside the white box. Scale bars, 200 μm (left) and 50 μm (right). **c**, Quantification of *Fos*-expressing neurons that co-express *Htr2c*, *Htr1b* or *Foxp2*. Data points represent the average number of cells counted per slice for each animal. Saline, $n = 5$ mice; hypertonic saline, $n = 5$ mice. Two-way ANOVA: treatment ($F_{2,24} = 22.72$, $P < 0.0001$); gene ($F_{1,24} = 7.671$, $P = 0.0107$); interaction ($F_{2,24} = 5.949$, $P = 0.0080$). All post hoc tests were performed using the Bonferroni correction, $P = 0.000552$. **d**, Co-localization of *Fos* with *Htr1b* transcripts in the LPBN after gastric loading of saline or hypertonic saline. Scale bar, 50 μm. **e**, Co-localization of *Fos* with *Foxp2* transcripts in the LPBN after gastric loading of saline or hypertonic saline. Scale bar, 50 μm. **f**, Quantification of the percentage of *Htr2c*-expressing neurons that co-express *Htr1b*, *Foxp2* or *Oxt*. Data points represent average percentages counted per slice for each animal ($n = 10$ mice). **g**, Co-localization of *Htr1b* with *Htr2c* transcripts in the LPBN. Left: low magnification picture; right: higher magnification of the area inside the white box. Scale bars, 200 μm (left) and 50 μm (right). **h**, Co-localization of *Foxp2* with *Htr2c* transcripts in the LPBN. Left: low magnification picture; right: higher magnification of the area inside the white box. Scale bars, 200 μm (left) and 50 μm (right). **i**, Co-localization of *Oxt* with *Htr2c* transcripts in the LPBN. Left: low magnification picture; right: higher magnification of the area inside the white box. Scale bars, 200 μm (left) and 50 μm (right). **j**, Representative cell-attached recording of an LPBN^{Htr2c} neuron after 7–8 d of control diet (top) or 7–8 d of sodium-deficient diet (bottom). **k**, Firing frequency of LPBN^{Htr2c} neurons in control-diet-fed mice (left) and sodium-deficient-diet-fed mice (right). Control diet, $n = 14$ cells; sodium-deficient diet, $n = 13$ cells. Control diet, 1.2 ± 0.4 Hz; sodium-deficient diet, 0.1 ± 0.1 Hz (two-tailed Mann-Whitney test, $P = 0.008$). **l**, Representative cell-attached recording of an LPBN^{Htr2c} neuron after furosemide and control diet treatment (top) or furosemide and sodium-deficient diet treatment (bottom). **m**, Firing frequency of LPBN^{Htr2c} neurons in control-diet-fed mice (left) and sodium-deficient-diet-fed mice (right). Furosemide (furo) + control diet, $n = 11$ cells; furosemide + sodium-deficient diet, $n = 10$ cells. Furosemide + control diet, 2.0 ± 0.3 Hz; furosemide + sodium-deficient diet, 0.6 ± 0.2 Hz (two-tailed Mann-Whitney test, $P = 0.0007$). All data are represented as mean ± s.e.m. ** $P < 0.01$, *** $P < 0.001$.

LPBN^{Htr2c} neurons are inhibited during sodium depletion. To target LPBN^{Htr2c} neurons, we generated an *Htr2c*-2A-iCre mouse line in which expression of the codon-improved Cre recombinase (iCre) is under the control of the endogenous regulatory sequences of the *Htr2c* gene (Extended Data Fig. 2a). The coding sequences of *Htr2c* and *iCre* were linked by a viral peptide bridge 2A sequence so that the two heterologous genes were initially transcribed from a single open reading frame and later segregated via a ribosomal-skip

mechanism¹⁸. PCR genotyping detected both the targeted *Htr2c*-2A-iCre and wild-type *Htr2c* alleles in female heterozygous *Htr2c*-2A-iCre mice (Extended Data Fig. 2b). Because *Htr2c* is located on the X chromosome, we observed only one band (targeted) in male hemizygous *Htr2c*-2A-iCre mice. Immunohistochemical analysis of *Htr2c*-2A-iCre activity using a tdTomato reporter revealed expression of *Htr2c* in the choroid plexus, a brain region that is known to express high levels of *Htr2c* (Extended Data Fig. 2c).

To then test whether LPBN^{Htr2c} neuronal activity is modulated by sodium depletion, we targeted LPBN^{Htr2c} neurons using Htr2c-2A-iCre::tdTomato mice. Cell-attached recordings were taken from targeted LPBN^{Htr2c} neurons from mice maintained 7–8 d on either a control diet (0.11% sodium) or a sodium-deficient diet. These diets differed only in sodium content and were otherwise identical in composition. Cells recorded from sodium-depleted mice showed a significant reduction in firing frequency compared to cells from mice that were maintained on a control diet (Fig. 1j,k), suggesting that LPBN^{Htr2c} neurons are inhibited during sodium depletion. We also recapitulated these results in Htr2c-2A-iCre mice injected with AAV-DIO-EYFP in the LPBN (Extended Data Fig. 3a–c) to control for any possible transient Cre expression during development. We obtained similar results with LPBN^{Htr2c} neurons from mice that were depleted of sodium by subcutaneous injections of furosemide (50 mg kg⁻¹) and given access to water and sodium-deficient diet for 1 d (Fig. 1l,m). Taken together, these results suggest that LPBN^{Htr2c} neurons are responsive to changes in bodily sodium content.

Stimulation of LPBN^{Htr2c} neurons reduces sodium intake. To test the functional relevance of LPBN^{Htr2c} neurons in regulating sodium intake, we established a sodium-depletion protocol to promote sodium appetite in mice (Fig. 2a). We unilaterally injected AAV-DIO-hM3Dq-mCherry into the LPBN of Htr2c-2A-iCre mice (LPBN^{Htr2c-hM3Dq} mice) to specifically activate LPBN^{Htr2c} neurons (Fig. 2b). We verified these constructs by current-clamp recordings. Applications of clozapine N-oxide (CNO) (5 μM) could depolarize membrane potential (5.2 ± 1.7 mV in 3/3 cells tested) and induce robust action potentials (Fig. 2c). We tested sodium-depleted LPBN^{Htr2c-hM3Dq} mice in a two-bottle assay, giving them a choice between distilled water and a solution containing 300 mM NaCl. In this condition, we found that CNO (1 mg kg⁻¹)-injected LPBN^{Htr2c-hM3Dq} mice showed a decrease in intake of 300 mM NaCl solution compared to saline-injected controls, while water intake was unchanged (Fig. 2d). We confirmed that CNO injections caused no differences in water intake or 300 mM NaCl intake in AAV-DIO-mCherry-injected Htr2c-2A-iCre mice that were deprived of sodium, validating that CNO injections alone do not alter sodium intake (Extended Data Fig. 4a,b).

Because chemogenetics offers limited temporal resolution, we tested whether optogenetic activation of LPBN^{Htr2c} neurons in a temporally specific manner could recapitulate the chemogenetic results. To this end, we unilaterally injected AAV-DIO-hChR2 (E123T/T159C)-EYFP (hereafter, ChETA_{TC}-EYFP) into the LPBN of Htr2c-2A-iCre mice that were deprived of sodium (Fig. 2e). Photostimulation of ChETA_{TC}-EYFP-expressing neurons (20 Hz, 10-ms pulses, 1-s duration) generated inward currents in voltage-clamp mode and action potentials in current-clamp mode (5/5 cells tested) (Fig. 2f). We then designed a closed-loop optogenetic protocol using a lickometer to deliver photostimulation (10 Hz, 10-ms pulses, 1-s duration) upon each lick. We tested AAV-DIO-ChETA_{TC}-EYFP-injected mice in a one-bottle assay (300 mM NaCl) and found that photostimulation locked to each lick could acutely and potently suppress sodium intake, whereas photostimulation had no effect in AAV-DIO-EYFP-injected control mice (Fig. 2g,h). Taken together, these results suggest that activation of LPBN^{Htr2c} neurons can rapidly suppress sodium intake during sodium depletion.

Inhibition of LPBN^{Htr2c} neurons promotes sodium intake. Having shown that activation of LPBN^{Htr2c} neurons significantly suppressed sodium intake, we next asked whether inhibiting the activity of these neurons could promote sodium intake. To this end, we injected AAV-DIO-hM4Di-mCherry bilaterally into the LPBN of Htr2c-2A-iCre mice (LPBN^{Htr2c-hM4Di} mice) (Fig. 3a). We validated this chemogenetic construct in situ by current-clamp recordings. Applications of CNO (5 μM) indeed hyperpolarized membrane potential (−5.8 ± 0.6 mV

in 11/13 cells tested) and silenced LPBN^{Htr2c} neurons (Fig. 3b). CNO-injected LPBN^{Htr2c-hM4Di} mice showed an increase in consumption of 300 mM NaCl solution in the two-bottle assay during sodium depletion, while leaving water intake unchanged (Fig. 3c). These data suggest that inhibition of LPBN^{Htr2c} neuronal activity can further accentuate sodium intake during sodium depletion.

To test whether inhibition of LPBN^{Htr2c} neuronal activity could drive sodium intake in a condition where sodium appetite is not as pronounced, we dehydrated LPBN^{Htr2c-hM4Di} mice (Fig. 3d) before testing them on the two-bottle assay. Again, CNO injections into LPBN^{Htr2c-hM4Di} mice during the dehydrated state increased sodium intake compared to saline-injected controls, while water intake did not change (Fig. 3e). Because both sodium depletion and dehydration result in hypovolemia, we tested mice under euvolemic conditions to determine whether LPBN^{Htr2c} neurons are necessary for the suppression of sodium appetite in normal circumstances (Fig. 3f). Interestingly, euvolemic CNO-injected LPBN^{Htr2c-hM4Di} mice showed increased 300 mM NaCl intake without a change in water intake (Fig. 3g). This increased salt intake was abolished when 300 mM KCl was used instead of NaCl (Fig. 3h) but was restored when mice were given 300 mM NaHCO₃ (Fig. 3i). These results demonstrate the specificity of these behaviors toward sodium. Because sodium intake is typically obtained through feeding instead of ingesting concentrated salt solutions, we tested whether inhibition of LPBN^{Htr2c} neuronal activity could also promote intake of food that contains sodium. We tested LPBN^{Htr2c-hM4Di} mice on a fast-refeeding protocol (Fig. 3j) using either a control diet or a sodium-deficient diet. CNO-injected LPBN^{Htr2c-hM4Di} mice showed an increase in food intake compared to saline-injected controls when offered a control diet (Fig. 3k). Remarkably, this apparently orexigenic effect was abolished when LPBN^{Htr2c-hM4Di} mice were instead offered a sodium-deficient diet. These data suggest that the increase in food intake caused by inhibition of LPBN^{Htr2c} neuronal activity is contingent on sodium being present in the diet. Finally, we confirmed that CNO injections caused no differences in food intake in AAV-DIO-mCherry-injected control mice on a fast-refeeding paradigm, indicating that CNO injections alone do not influence the intake of salt-containing food (Extended Data Fig. 4a,c).

Stimulation of LPBN^{Htr2c} neurons has effects unrelated to sodium intake. Although inhibition of LPBN^{Htr2c} neuronal activity produced effects that were specific to sodium, LPBN^{Htr2c-hM3Dq} mice displayed effects that were independent of sodium. CNO-injected LPBN^{Htr2c-hM3Dq} mice showed both decreased 300 mM NaCl intake and water intake during dehydrated conditions, compared to saline-injected controls (Extended Data Fig. 5a,b). These data suggest that, although LPBN^{Htr2c} neurons can decrease sodium intake during dehydration, LPBN^{Htr2c} neurons or a subset of them are also capable of reducing water intake under certain circumstances. We also found that activation of LPBN^{Htr2c} neurons caused sodium-independent decreases in food intake (Extended Data Fig. 5a,c). We speculated that these results might have been mediated by activation of calcitonin gene-related peptide (CGRP) neurons (LPBN^{CGRP} neurons), which were shown to reduce water intake during dehydration¹⁷ and to exert anorexigenic effects¹⁹. Indeed, we found that a subset (34% ± 3%) of LPBN^{CGRP} neurons overlapped with LPBN^{Htr2c} neurons (Extended Data Fig. 6a,b). However, it is unlikely that LPBN^{CGRP} neurons were responsible for mediating natriorexigenic effects, as inhibition of these neurons reduced malaise^{19,20} or increased meal size²¹, which would cause sodium-independent increases in ingestion. Furthermore, activation of LPBN^{CGRP} neurons did not decrease 300 mM NaCl intake during dehydration¹⁷. Notably, during our optogenetic experiments, we used a photostimulation frequency of 10 Hz to avoid inducing malaise through LPBN^{CGRP} neurons, as they have been shown to induce little malaise at 20 Hz¹⁹.

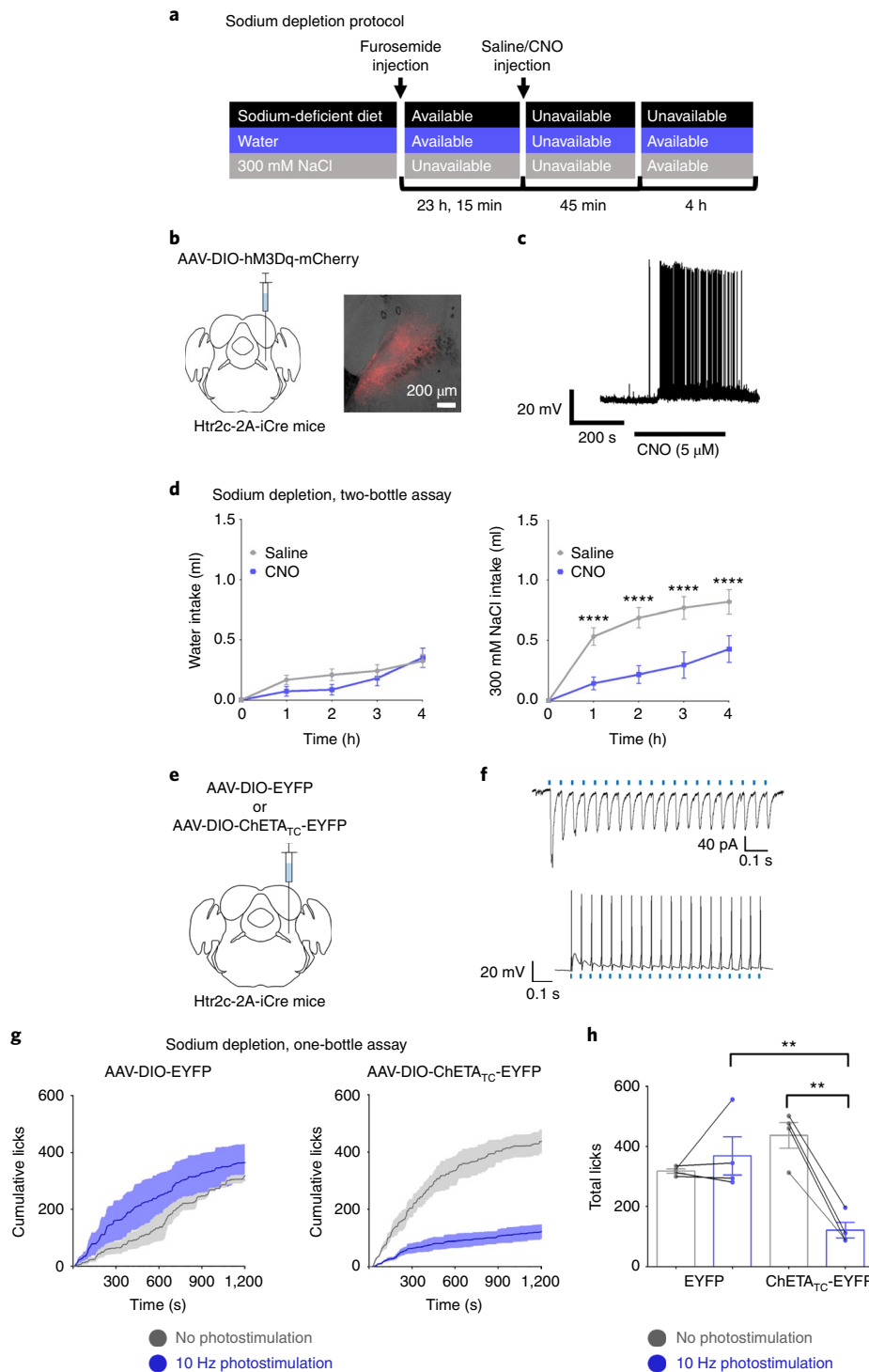


Fig. 2 | Activation of LPBN^{Htr2c} neurons suppresses sodium intake. **a**, Schematic illustration showing the schedule for sodium depletion. **b**, Left: unilateral injection of AAV5-hSyn-DIO-hM3Dq-mCherry into the LPBN of Htr2c-2A-iCre mice. Right: representative image of injection site. Scale bar, 200 μ m. **c**, DREADDs validated by current-clamp recordings. **d**, Water intake during sodium depletion: two-way repeated-measures ANOVA: time ($F_{4,40} = 33.11$, $P < 0.0001$); treatment ($F_{1,10} = 0.8369$, $P = 0.3818$); interaction ($F_{4,40} = 1.712$, $P = 0.1663$). 300 mM NaCl intake during sodium depletion: two-way repeated-measures ANOVA: time ($F_{4,40} = 68.77$, $P < 0.0001$); treatment ($F_{1,10} = 10.57$, $P = 0.0089$); interaction ($F_{4,40} = 7.546$, $P = 0.0001$) ($n = 11$). **e**, Unilateral injection of AAV5-EF1a-DIO-ChETA_{TC}-EYFP or AAV5-EF1a-DIO-EYFP into the LPBN of Htr2c-2A-iCre mice. **f**, Photostimulation of ChETA_{TC}-expressing neurons (20 Hz, 10-ms pulses, 1-s duration) efficiently drives photocurrents and action potentials in voltage-clamp (top) and current-clamp (bottom) recordings, respectively. **g**, Closed-loop optogenetic photostimulation of LPBN^{Htr2c} neurons during a one-bottle assay (300 mM NaCl) after sodium depletion. Cumulative licks of 300 mM NaCl are shown for AAV5-EF1a-DIO-EYFP-injected mice (left) and AAV5-EF1a-DIO-ChETA_{TC}-EYFP-injected mice (right). EYFP, $n = 4$ mice; ChETA_{TC}-EYFP, $n = 4$ mice. **h**, Total licks measured in AAV5-EF1a-DIO-EYFP-injected mice and AAV5-EF1a-DIO-ChETA_{TC}-EYFP-injected mice at the end of the experiment. Two-way repeated-measures ANOVA: photostimulation ($F_{1,6} = 14.26$, $P = 0.0092$); virus ($F_{1,6} = 1.986$, $P = 0.2085$); interaction ($F_{1,6} = 27.37$, $P = 0.002$). EYFP, $n = 4$ mice; ChETA_{TC}-EYFP, $n = 4$ mice. All post hoc tests were performed using the Bonferroni correction. All data are represented as mean \pm s.e.m. ** $P < 0.01$, **** $P < 0.0001$.

Glutamatergic projections from LPBN^{Htr2c} neurons to the central amygdala suppress sodium appetite. To reveal the downstream circuitry of LPBN^{Htr2c} neurons, we injected AAV-DIO-EYFP into the LPBN of Htr2c-2A-iCre mice (Fig. 4a and Extended Data Fig. 7a). Among the brain regions that have been implicated in regulating sodium appetite, we found dense projections to the bed nucleus of the stria terminalis (BNST), the central amygdala (CeA), the paraventricular hypothalamus (PVH), the parvocellular part of the ventroposterior thalamus (VPPC) and the median preoptic nucleus (MnPO). We also noted projections toward the ventromedial hypothalamus (VMH) and insular cortex (IC) but excluded these areas from further analysis because the VMH has little relevance to sodium appetite and the IC received sparse projections. To identify a candidate site for in vivo terminal photostimulation, we first carried out channelrhodopsin-assisted circuit mapping (CRACM) to identify functional connectivity between LPBN^{Htr2c} neurons and downstream regions. We bilaterally injected AAV-DIO-hChR2 (H134R)-mCherry into the LPBN of Htr2c-2A-iCre mice (Fig. 4b and Extended Data Fig. 7b) and then performed whole-cell patch-clamp recordings at target sites to record photo-excitatory postsynaptic currents (pEPSCs) and photo-inhibitory postsynaptic currents (pIPSCs) in voltage-clamp modes at -60 mV and -10 mV, respectively. We failed to detect either pEPSCs or pIPSCs in the dorsal BNST (dBNST), ventral BNST (vBNST) or PVH (Extended Data Fig. 7b). Contrary to this, we detected pEPSCs to the VPPC (1/11 neurons recorded; 9%), MnPO (1/9 neurons recorded; 11%) and CeA (14/25 neurons recorded; 56%) (Fig. 4b and Extended Data Fig. 7b). We also detected pIPSCs in the CeA (3/24 neurons recorded; 13%) but speculate that these are not monosynaptic owing to the longer response latencies (17.7 ± 0.8 ms; $n = 3$). Application of kynurenic acid (1 mM) abolished pEPSCs in the CeA, but, upon washout, pEPSCs were recovered (4/4 neurons recorded; 100%), suggesting that the pEPSCs were glutamatergic (Fig. 4c). Given the abundant connectivity between LPBN^{Htr2c} neurons and the CeA, we targeted this projection for in vivo stimulation by unilaterally injecting AAV-DIO-hChR2 (H134R)-mCherry into the LPBN of Htr2c-2A-iCre mice and implanting optic fibers ipsilaterally over the CeA (Fig. 4d,e). By using a closed-loop optogenetic design to deliver photostimulation (10 Hz, 10-ms pulses, 1-s duration) upon each lick, we found that activating the LPBN^{Htr2c} \rightarrow CeA projection was sufficient to suppress sodium appetite in sodium-depleted mice (Fig. 4f,g). Together, these results suggest that LPBN^{Htr2c} neurons are able to suppress sodium appetite via glutamatergic projections to the CeA.

Htr2c agonist directly inhibits LPBN^{Htr2c} neuronal activity via K_{ATP} channels. To investigate the function of Htr2c on LPBN neurons at the electrophysiological level, we made whole-cell patch-clamp recordings from tdTomato-expressing LPBN^{Htr2c} neurons. Application of mCPP (4 μ M), an Htr2c agonist, led to hyperpolarization in a subset (10/57 cells tested; 17.5%) of LPBN^{Htr2c} neurons (Fig. 5a and Extended Data Fig. 8). This effect was accompanied by a decrease in input resistance with a reversal potential of -86.9 ± 4.6 mV ($n = 10$), suggesting the involvement of putative potassium ion (K^+) conductance (Fig. 5b–d). We hypothesized that this increase in K^+ conductance may have been through ATP-sensitive K^+ (K_{ATP}) channels. To test this, we pretreated neurons with tolbutamide, a K_{ATP} channel blocker, before application of mCPP. No hyperpolarizations in response to mCPP were observed in this condition (Fig. 5e,g), and input resistance was not affected by mCPP (Fig. 5f,g). These data suggest that K_{ATP} channels mediate the hyperpolarization of LPBN neurons upon Htr2c activation. Notably, tolbutamide alone caused a depolarization of membrane potential (5.2 ± 0.9 mV) and an increase of input resistance in most cells tested ($n = 13/20$) (Fig. 5e–g), suggesting that K_{ATP} channels may contribute to the resting membrane potential (RMP) of LPBN^{Htr2c} neurons. Because mCPP might also have affinity for Htr1b, we pretreated slices with SB216641 (200 nM), an Htr1b antagonist. The effects of mCPP persisted in this condition, suggesting that the hyperpolarization was independent of Htr1b (Extended Data Fig. 9a,b). Pretreatment of slices with synaptic blockers (0.5 μ M TTX, 1 mM kynurenic acid, 50 μ M picrotoxin) also did not change the effects of mCPP, suggesting that these effects were postsynaptic (Extended Data Fig. 9c,d). A previous report suggested that a subset of neurons within the PVH projecting to the LPBN are calorically responsive²². Thus, we tested whether a similar phenomenon could be observed in LPBN^{Htr2c} neurons. However, fasting mice for 18 h did not change the amplitude or proportion of responses to mCPP. These data suggest that LPBN Htr2c responses are not influenced by changes in caloric state (Extended Data Fig. 9e–g).

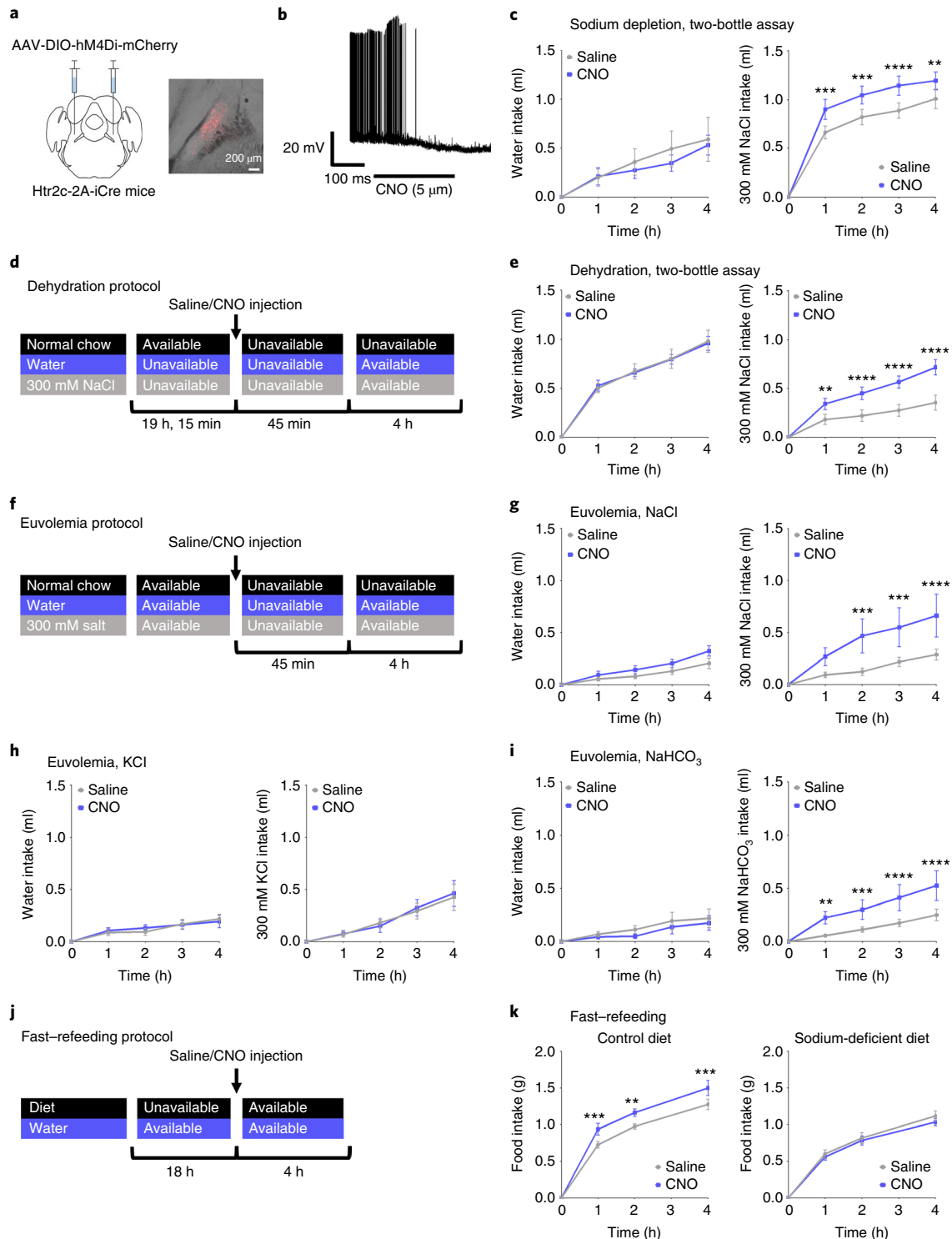
Deletion of Htr2c in LPBN reduces sodium intake during hypovolemia. To test the physiological role of Htr2c in the LPBN in regulating sodium intake, we generated LPBN-specific knockout mice by injecting AAV-CMV-Cre-GFP directly into the LPBN of Htr2c^{lox/Y} mice (LPBN^{Htr2cKO} mice) (Fig. 6a). We confirmed successful deletion of Htr2c in the LPBN through fluorescence in situ hybridization (Fig. 6b,c). Subjecting LPBN^{Htr2cKO} mice to two-bottle choice experiments revealed that AAV-CMV-Cre-GFP-injected mice had decreased intake of 300 mM NaCl solution in both the

Fig. 3 | Inhibition of LPBN^{Htr2c} neurons increases sodium intake. **a**, Left: bilateral injection of AAV2-hSyn-DIO-hM4Di-mCherry into the LPBN of Htr2c-2A-iCre mice. Right: representative image of the injection site. Scale bar, 200 μ m. **b**, DREADDs validated through current-clamp recordings. **c**, Water intake during sodium depletion: two-way repeated-measures ANOVA: time ($F_{4,40} = 33.11$, $P < 0.0001$); treatment ($F_{1,10} = 0.8369$, $P = 0.3818$); interaction ($F_{4,40} = 1.712$, $P = 0.1663$). 300 mM NaCl intake during sodium depletion: two-way repeated-measures ANOVA: time ($F_{4,40} = 68.77$, $P < 0.0001$); treatment ($F_{1,10} = 10.57$, $P = 0.0089$); interaction ($F_{4,40} = 7.546$, $P = 0.0001$) ($n = 11$). **d**, Schematic illustration showing the schedule for dehydration. **e**, Water intake during dehydration: two-way repeated-measures ANOVA: time ($F_{4,44} = 127.3$, $P < 0.0001$); treatment ($F_{1,11} = 0.001088$, $P = 0.9743$); interaction ($F_{4,44} = 0.09926$, $P = 0.9821$). 300 mM NaCl intake during dehydration: two-way repeated-measures ANOVA: time ($F_{4,44} = 59.29$, $P < 0.0001$); treatment ($F_{1,11} = 9.495$, $P = 0.0104$); interaction ($F_{4,44} = 8.926$, $P < 0.0001$) ($n = 12$). **f**, Schematic illustration showing the schedule for euvoolemia tests. **g**, Water intake: two-way repeated-measures ANOVA: time ($F_{4,28} = 29.26$, $P < 0.0001$); treatment ($F_{1,7} = 4.019$, $P = 0.085$); interaction ($F_{4,28} = 1.334$, $P = 0.282$). 300 mM NaCl intake: two-way repeated-measures ANOVA: time ($F_{4,28} = 12.04$, $P < 0.0001$); treatment ($F_{1,7} = 5.615$, $P = 0.0496$); interaction ($F_{4,28} = 4.625$, $P < 0.0054$) ($n = 8$). **h**, Water intake: two-way repeated-measures ANOVA: time ($F_{4,28} = 19.15$, $P < 0.0001$); treatment ($F_{1,7} = 0.01671$, $P = 0.9008$); interaction ($F_{4,28} = 0.5804$, $P = 0.6793$). 300 mM KCl intake: two-way repeated-measures ANOVA: time ($F_{4,28} = 13.26$, $P < 0.0001$); treatment ($F_{1,7} = 0.02963$, $P = 0.8682$); interaction ($F_{4,28} = 0.4732$, $P = 0.7550$) ($n = 8$). **i**, Water intake: two-way repeated-measures ANOVA: time ($F_{4,28} = 8.521$, $P < 0.0001$); treatment ($F_{1,7} = 0.5266$, $P = 0.4916$); interaction ($F_{4,28} = 0.2829$, $P = 0.8866$). 300 mM NaHCO₃ intake: two-way repeated-measures ANOVA: time ($F_{4,28} = 14.14$, $P < 0.0001$); treatment ($F_{1,7} = 8.089$, $P = 0.0249$); interaction ($F_{4,28} = 6.304$, $P = 0.0010$) ($n = 8$). **j**, Schematic illustration showing the schedule for the fast-refeeding protocol. **k**, Left: control diet food intake, $n = 8$: two-way repeated-measures ANOVA: time ($F_{3,21} = 226.7$, $P < 0.0001$); treatment ($F_{1,7} = 13.06$, $P = 0.0086$); interaction ($F_{3,21} = 4.987$, $P = 0.0091$). Right: sodium-deficient diet food intake, $n = 12$: two-way repeated-measures ANOVA: time ($F_{3,33} = 216.2$, $P < 0.0001$); treatment ($F_{1,11} = 0.7438$, $P = 0.4069$); interaction ($F_{3,33} = 0.4746$, $P = 0.7021$). All post hoc tests were performed using the Bonferroni correction. All data are represented as mean \pm s.e.m. ** $P < 0.01$, *** $P < 0.001$, **** $P < 0.0001$.

sodium-depleted state and the dehydrated state compared to AAV-CMV-GFP-injected controls (Fig. 6d,e). However, food intake was unaltered in LPBN^{Htr2c}KO mice regardless of the diet used (Fig. 6f). Taken together, these results suggest that Htr2c can inhibit LPBN neurons and thus act to disinhibit sodium intake, but plays no physiological role in regulating caloric appetite.

We speculate that the discrepancy between results obtained from LPBN^{Htr2c}KO mice and direct activation of LPBN^{Htr2c} neurons was presumably due to the degree of activation that occurs on these neurons. Removal of *Htr2c* would only be expected to have

noticeable effects in conditions where serotonin is present, whereas the effects of chemogenetic modulation are not contingent upon this. Thus, serotonin release onto these neurons presumably occurs during conditions of hypovolemia (that is, by sodium depletion or dehydration) but not during fasting, which might account for the lack of effect on food intake in LPBN^{Htr2c}KO mice, despite the presence of sodium in the diet. We tested this hypothesis by comparing the intake of water and 300 mM NaCl solution in euvoletic mice. In this state, we observed no difference in these measures between LPBN^{Htr2c}KO mice and control mice (Fig. 6g), suggesting that the



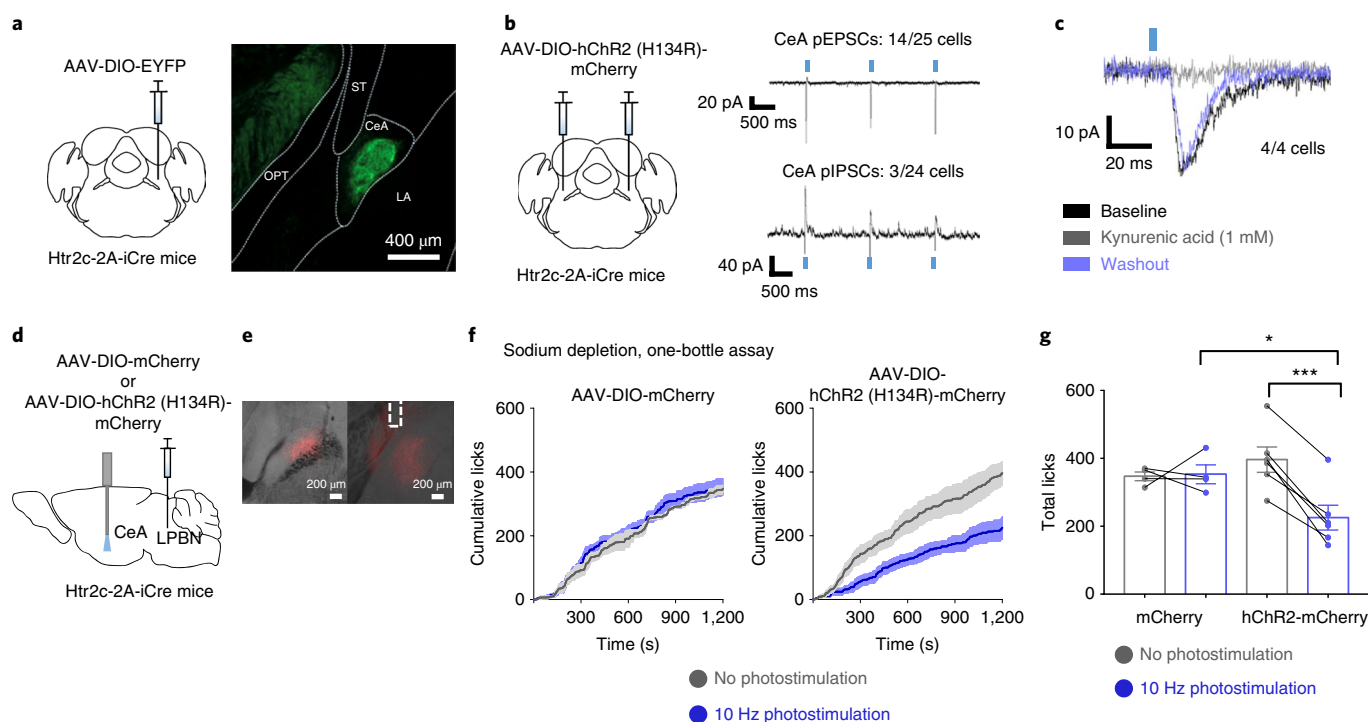


Fig. 4 | Stimulation of the LPBN^{Htr2c} → CeA projection suppresses sodium intake. **a**, Schematic of the experiment. Left: unilateral injection of AAV5-EF1a-DIO-EYFP into the LPBN of Htr2c-2A-iCre mice to visualize axonal projections. Right: EYFP labelling of axons in the CeA. CeA, central amygdala; LA, lateral amygdala; OPT, optic tract; ST, stria terminalis. Scale bar, 400 μm ($n = 7$ mice). **b**, Schematic of the experiment. Left: bilateral injection of AAV2-EF1a-DIO-hChR2 (H134R)-mCherry into the LPBN of Htr2c-2A-iCre mice. Right: voltage-clamp recordings taken at the CeA. The blue rectangles indicate times of photostimulation. **c**, Kynurenic acid (1 mM) application abolished pEPSCs at the CeA. Blue rectangle indicates the time of photostimulation. **d**, Schematic of the experiment. Unilateral injection of AAV2-EF1a-DIO-hChR2 (H134R)-mCherry into the LPBN of Htr2c-2A-iCre mice and implantation of an optic fiber ipsilaterally over the CeA. **e**, Representative image of the injection site (left) and representative image of the fiber implantation site (right). Dashed lines indicate fiber placement. Scale bars, 200 μm. **f**, Closed-loop optogenetic photostimulation of LPBN^{Htr2c} neurons during a one-bottle assay (300 mM NaCl) after sodium depletion. Cumulative licks of 300 mM NaCl are shown in AAV2-EF1a-DIO-mCherry-injected mice (left) and AAV2-EF1a-DIO-hChR2 (H134R)-mCherry-injected mice (right). mCherry, $n = 4$ mice; hChR2-mCherry, $n = 6$ mice. **g**, Total licks measured in AAV2-EF1a-DIO-mCherry-injected mice and AAV2-EF1a-DIO-hChR2 (H134R)-mCherry-injected mice at the end of the experiment. Two-way repeated-measures ANOVA: photostimulation ($F_{1,8} = 15.61$, $P = 0.0042$); virus ($F_{1,8} = 0.7701$, $P = 0.4058$); interaction ($F_{1,8} = 17.97$, $P = 0.00028$). mCherry, $n = 4$ mice; hChR2-mCherry, $n = 6$ mice. All post hoc tests were performed using the Bonferroni correction. All data are represented as mean \pm s.e.m. * $P < 0.05$, *** $P < 0.001$.

effects of *Htr2c* deletion in the LPBN are dependent on the hypovolemic state.

Finally, to identify sources of serotonin for LPBN^{Htr2c} neurons, we injected wild-type mice with retrobeads (Extended Data Fig. 10a) and then counterstained upstream-labeled sites for serotonin (5-HT). Interestingly, we found co-localization of 5-HT and retrobead-labeled cells in the dorsal raphe (DR) nucleus and the median raphe (MnR) nucleus (Extended Data Fig. 10b), suggesting that these raphe nuclei might be capable of modulating the LPBN neurons through serotonergic projections.

Discussion

Maintenance of sodium content and body fluid volume is essential for survival and growth. Depletion of sodium is sensed through hypovolemia, which results in both increased retention of sodium and increased ingestion of sodium, the latter of which manifests as sodium appetite. However, previous studies have consistently reported a delay between the onset of hypovolemia and sodium appetite, leading to formulation of the ‘disinhibition hypothesis’ (ref. 23), which proposed the relief of sodium appetite from inhibitory mechanisms. Although previous studies showed inhibitory influences over sodium appetite, whether removal of any of those influences can drive increased sodium appetite during euvoletic conditions has remained contentious. Here we describe a subpopulation of neurons in the LPBN that suppress sodium appetite.

Animals tend to avoid ingesting high concentrations of sodium under normal circumstances, and our results suggest that LPBN^{Htr2c} neurons might be a central substrate that facilitates this suppression of sodium appetite. Furthermore, we showed that inhibition of these neurons was indeed able to drive sodium appetite, independently of thirst, even during euvoletic conditions. Our results were not restricted to sodium solutions but also extended to sodium-containing foods, suggesting that certain aspects of appetite regulation by the LPBN might be coupled to osmoregulation. This finding was somewhat surprising because LPBN lesion studies showed either no increase⁸ or reduced sodium appetite⁹, which further highlights the heterogeneity of LPBN neurons and the need for genetic segregation of their subpopulations.

Recent studies provided evidence that synergy between aldosterone and angiotensin II signaling underlie the promotion of sodium appetite⁴. Our results suggest that disinhibition of sodium appetite from the influence of LPBN^{Htr2c} neurons might also play an important complementary role. We note that synergy and disinhibition were not mutually exclusive mechanisms because the activity of LPBN^{Htr2c} neurons might also be modulated by aldosterone and angiotensin II signaling. Indeed, aldosterone-sensitive 11 β -hydroxysteroid dehydrogenase type 2 (HSD2) neurons within the nucleus tractus solitarius (NTS^{HSD2} neurons), which are considered the neural substrate for aldosterone signaling, have been shown to project to the LPBN^{3,4}. However, we find it unlikely that

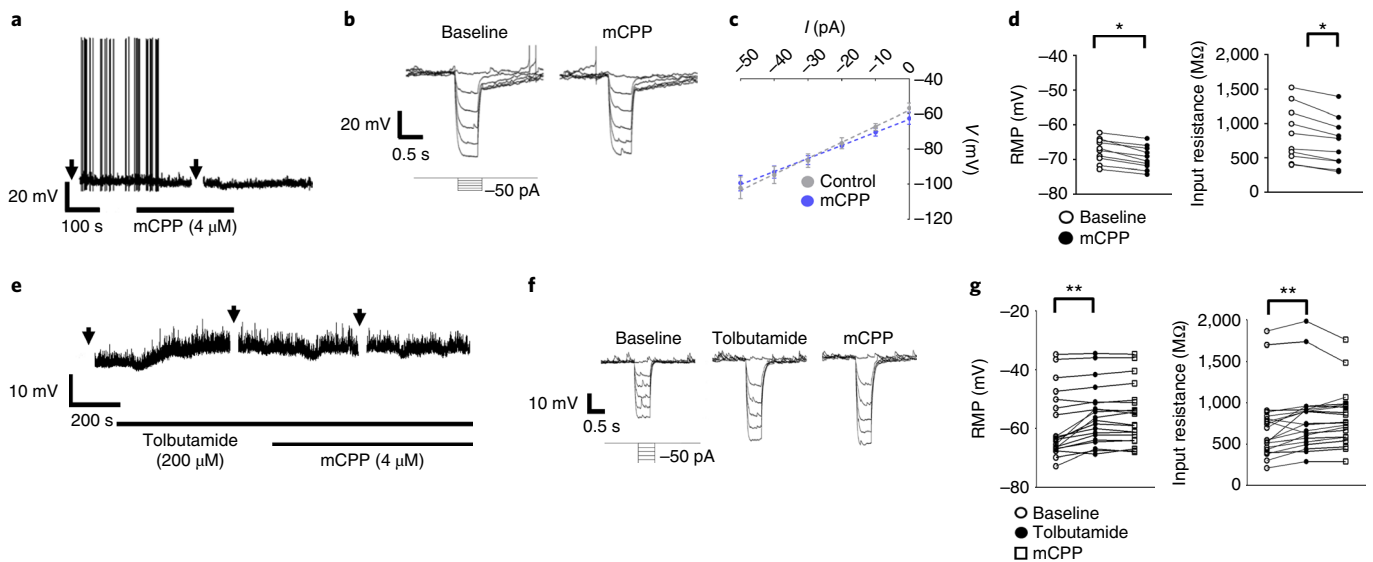


Fig. 5 | Htr2c inhibits LPBN neurons via K_{ATP} channels. **a**, Representative current-clamp recording of an LPBN^{Htr2c} neuron, showing hyperpolarization in response to mCPP. Arrows indicate the time at which current steps were applied. **b**, Voltage deflections in response to hyperpolarizing currents from the same neuron, showing decreased input resistance in response to mCPP. Current steps in the trace were made in 10-pA increments from -50 pA to 0 pA. **c**, Averaged current-voltage (I - V) plot across responsive neurons, showing decreased input resistance in response to mCPP. Reversal potential was calculated to be -86.9 ± 4.6 mV ($n = 6$ cells). **d**, Change in RMP and input resistance across mCPP-responsive neurons; two-tailed Wilcoxon signed-rank test, $P = 0.002$ ($n = 10$ cells). **e**, Representative current-clamp recording of an LPBN^{Htr2c} neuron. Neurons depolarize in response to tolbutamide and no longer respond to mCPP. Arrows indicate the time at which current steps were applied. **f**, Voltage deflections in response to hyperpolarizing currents from the same neuron, showing increased input resistance in response to tolbutamide but no change during mCPP application. Current steps in the trace were made in 10-pA increments from -50 pA to 0 pA. **g**, Individual data points for RMP (left) and input resistance (right) before and during tolbutamide application in all recorded cells. Mean depolarization resulting from tolbutamide alone was 3.5 ± 0.8 mV. RMP: repeated-measures ANOVA with a Greenhouse-Geisser correction ($F_{1,127,21,41} = 19.059$, $P = 0.001$). Input resistance: repeated-measures ANOVA with a Greenhouse-Geisser correction ($F_{1,376,26,51} = 8.627$, $P = 0.0035$). All post hoc tests were performed using the Bonferroni correction ($n = 20$ cells). All data are represented as mean \pm s.e.m. * $P < 0.05$, ** $P < 0.01$.

these neurons mediate their effects by directly terminating on LPBN^{Htr2c} neurons, because NTS^{HSD2} neurons have been shown to be Phox2b-positive neurons²⁴, which are selectively glutamatergic²⁵. NTS^{HSD2} neurons project instead to Foxp2 neurons within the LPBN (LPBN^{Foxp2} neurons), putatively sodium appetite-promoting neurons^{3,4}, which we found not to overlap significantly with LPBN^{Htr2c} neurons in the central LPBN. The presence of both sodium appetite-promoting and appetite-suppressing neurons in the LPBN is of interest, raising the possibility that these subpopulations might even interact with each other.

We found that LPBN^{Htr2c} neurons were responsive to bodily sodium content, responding to high concentrations of gastrically loaded sodium and scaling down their activity during sodium depletion. Although it is likely that LPBN^{Htr2c} neurons receive baroreceptive information via the NTS⁸, it is well known that PBN neurons, particularly those in the waist region, are responsive to tastants^{26,27}. Previous studies regarding the detection of salt tastants showed that the detection of aversive concentrations of salt occurred in an amiloride-insensitive, non-sodium-specific manner²⁸. This raises the possibility that LPBN^{Htr2c} neurons mediate aversion toward high concentrations of salt in general. However, we find this to be unlikely, as we found that chemogenetic inhibition of LPBN^{Htr2c} neurons selectively increased intake of sodium salts but not potassium salts. Our results suggest that animals are able to translate decreased activity of LPBN^{Htr2c} neurons into a sodium-specific behavior, as opposed to a generalized intake of all salts. Nevertheless, the nature of the information conveyed by LPBN^{Htr2c} neurons appears to be sufficient to regulate sodium intake on a rapid time scale during sodium depletion, as seen in our optogenetic experiments.

Our experiments showed that these rapid effects appear to be mediated by projections to the CeA, which has been anatomically

implicated in regulating sodium appetite^{29,30}. We also found that LPBN^{Htr2c} neurons project to the vBNST, which has been shown to be a functionally relevant target of the angiotensin II receptor 1a (AT1a)-expressing neurons within the subfornical organ (SFO^{AT1a} neurons)² and NTS^{HSD2} neurons⁴, which both promote sodium appetite. Although this raised the attractive possibility that LPBN^{Htr2c} neurons might reduce sodium appetite by sending inhibitory projections to vBNST neurons innervated by SFO^{AT1a} and NTS^{HSD2} neurons, we failed to detect pIPSCs from LPBN^{Htr2c} neurons to vBNST neurons. In addition, the absence of pEPSCs from LPBN^{Htr2c} neurons to vBNST neurons likely ruled out the possibility that LPBN^{Htr2c} neurons inhibit vBNST neurons via excitation of interneurons. Although we cannot rule out the possibility that LPBN^{Htr2c} neurons might be able to influence the vBNST on a slower time scale via neuromodulators, this would not account for the rapid effects observed from our closed-loop optogenetic stimulation of LPBN^{Htr2c} neurons. Nevertheless, given the dense GABAergic projections between the CeA and vBNST^{31,32}, the signals from SFO^{AT1a} and NTS^{HSD2} neurons possibly act antagonistically to those from LPBN^{Htr2c} neurons, at the downstream level between the CeA and vBNST. Identifying whether the SFO^{AT1a} \rightarrow vBNST or NTS^{HSD2} \rightarrow vBNST projections are able to promote sodium intake despite LPBN^{Htr2c} neuronal activation will also be informative regarding the hierarchy and interplay between these sodium appetite-regulating populations. Finally, we noted a strong projection to the dBNST, which was recently implicated in conveying chemosensory signals related to sodium³³. However, we failed to detect any functional connectivity between dBNST and LPBN^{Htr2c} neurons through CRACM.

Involvement of serotonin in regulating sodium appetite through actions at the LPBN has been known from previous studies^{13,14}. However, the exact electrophysiological manifestations and

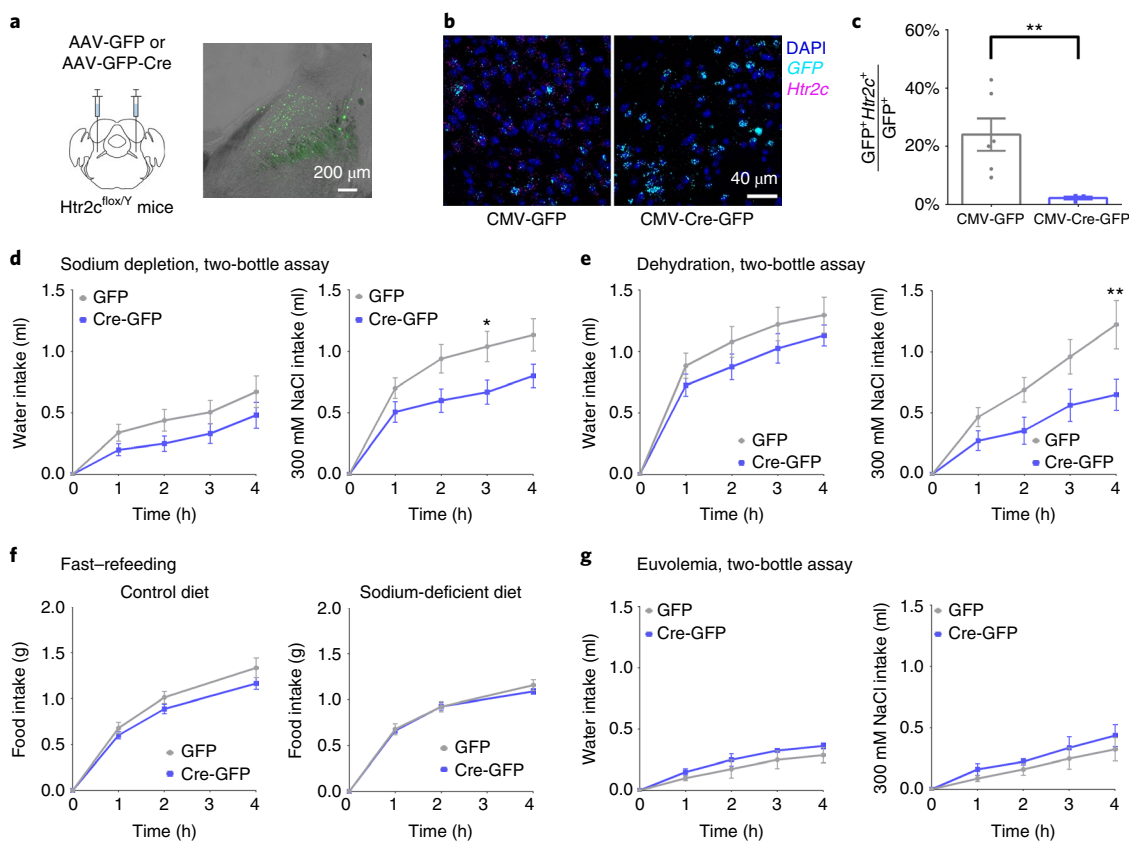


Fig. 6 | *Htr2c* in the LPBN is necessary to disinhibit sodium appetite during hypovolemia. **a**, Schematic of the experiment. Left: bilateral injections of either AAV5-CMV-GFP or AAV5-CMV-Cre-GFP into *Htr2c*^{fllox/y} mice. Right: representative image of the injection site. Scale bar, 200 μ m. **b**, Representative images validating knockout of *Htr2c* by in situ hybridization. Scale bar, 40 μ m. **c**, Quantification of *Htr2c* knockout. Two-tailed Mann-Whitney test, $P=0.0095$. CMV-GFP, $n=6$ mice; CMV-Cre-GFP, $n=4$ mice. **d**, Water intake during sodium depletion: two-way repeated-measures ANOVA: time ($F_{4,60}=39.08$, $P<0.0001$); treatment ($F_{1,15}=2.092$, $P=0.1686$); interaction ($F_{4,60}=1.389$, $P=0.2485$). 300 mM NaCl intake during sodium depletion: two-way repeated-measures ANOVA: time ($F_{4,60}=101.3$, $P<0.0001$); treatment ($F_{1,15}=4.521$, $P=0.0505$); interaction ($F_{4,60}=4.141$, $P=0.005$). CMV-GFP, $n=9$ mice; CMV-Cre-GFP, $n=8$ mice. **e**, Water intake during dehydration: two-way repeated-measures ANOVA: time ($F_{4,60}=140.1$, $P<0.0001$); treatment ($F_{1,15}=1.249$, $P=0.2813$); interaction ($F_{4,60}=1.024$, $P=0.4021$). 300 mM NaCl intake during dehydration: two-way repeated-measures ANOVA: time ($F_{4,60}=48.04$, $P<0.0001$); treatment ($F_{1,15}=5.117$, $P=0.039$); interaction ($F_{4,60}=4.276$, $P=0.0041$). CMV-GFP, $n=9$ mice; CMV-Cre-GFP, $n=8$ mice. **f**, Left: control diet food intake: two-way repeated-measures ANOVA: time ($F_{3,45}=302.9$, $P<0.0001$); treatment ($F_{1,15}=1.976$, $P=0.1802$); interaction ($F_{3,45}=1.405$, $P=0.2538$). Right: sodium-deficient diet food intake: two-way repeated-measures ANOVA: time ($F_{3,45}=465.2$, $P<0.0001$); treatment ($F_{1,15}=0.1966$, $P=0.6638$); interaction ($F_{3,45}=0.5274$, $P=0.6657$). CMV-GFP, $n=9$ mice; CMV-Cre-GFP, $n=8$ mice. **g**, Water intake during euvoemia: two-way repeated-measures ANOVA: time ($F_{4,24}=36.98$, $P<0.0001$); treatment ($F_{1,6}=1.254$, $P=0.3056$); interaction ($F_{4,24}=0.573$, $P=0.6848$). 300 mM NaCl intake during euvoemia: two-way repeated-measures ANOVA: time ($F_{4,24}=25.79$, $P<0.0001$); treatment ($F_{1,6}=0.9208$, $P=0.3743$); interaction ($F_{4,24}=0.5215$, $P=0.7208$). CMV-GFP, $n=4$ mice; CMV-Cre-GFP, $n=4$ mice. All post hoc tests were performed using the Bonferroni correction. All data are represented as mean \pm s.e.m. * $P<0.05$, ** $P<0.01$.

physiological relevance of these effects were not explored. We found that activation of *Htr2c* causes inhibition of LPBN^{Htr2c} neurons, suggesting that serotonergic signaling within the LPBN may serve to inhibit LPBN^{Htr2c} neurons in a certain context. Because *Htr2c* is considered an excitatory receptor, which is linked to G_q proteins, this result was somewhat surprising. However, previous reports suggested that *Htr2c* is able to engage both G_i- and G_q-related responses, as measured by decreases in cAMP production and chloride currents, which were abolished by pertussis toxin (PTX) and anti-G_o nucleotides, respectively^{34,35}. Furthermore, G_i signaling has been linked to activation of K_{ATP} channels in cardiac myocytes³⁶. The decrease in sodium appetite during hypovolemia, by conditionally knocking out *Htr2c* from the LPBN (LPBN^{Htr2cKO} mice), suggests that ECF volume may regulate serotonergic signaling in the LPBN, which in turn controls sodium intake by modulation of LPBN^{Htr2c} neuronal activity. We found serotonergic projections to the LPBN from the DR and MnR, consistent with other reports^{37,38}. The MnR is of particular interest because electrical stimulation of MnR has

been shown to increase blood pressure, which was attenuated in the presence of an inhibitor of tryptophan hydroxylase³⁹. On the other hand, electrical stimulation of the DR was shown to bidirectionally modulate blood pressure in a serotonin-independent manner. Thus, serotonergic cells in the MnR might possibly engage neural circuitry to defend against hypovolemia, with an appropriate behavioral output being increased sodium intake. In this model, serotonin release from the MnR onto the LPBN signals hypovolemia, which would act to disinhibit sodium appetite by acting on LPBN^{Htr2c} neurons. Detailed understanding of how blood pressure and bodily sodium content regulate serotonergic signaling and LPBN^{Htr2c} neuronal activity might be key in the development of novel antihypertensive agents via suppression of sodium appetite.

Online content

Any methods, additional references, Nature Research reporting summaries, source data, extended data, supplementary information, acknowledgements, peer review information; details of author

contributions and competing interests; and statements of data and code availability are available at <https://doi.org/10.1038/s41593-019-0573-2>.

Received: 16 March 2018; Accepted: 9 December 2019;
Published online: 20 January 2020

References

- Wagman, W. Sodium chloride deprivation: development of sodium chloride as a reinforcement. *Science* **140**, 1403–1404 (1963).
- Matsuda, T. et al. Distinct neural mechanisms for the control of thirst and salt appetite in the subfornical organ. *Nat. Neurosci.* **20**, 230–241 (2017).
- Jarvie, B. C. & Palmiter, R. D. HSD2 neurons in the hindbrain drive sodium appetite. *Nat. Neurosci.* **20**, 167–169 (2017).
- Resch, J. M. et al. Aldosterone-sensing neurons in the NTS exhibit state-dependent pacemaker activity and drive sodium appetite via synergy with angiotensin II signaling. *Neuron* **96**, 190–206 (2017).
- Oka, Y., Butnaru, M., von Buchholtz, L., Ryba, N. J. & Zuker, C. S. High salt recruits aversive taste pathways. *Nature* **494**, 472–475 (2013).
- de Oliveira, L. B., Callera, J. C., De Luca, L. A. Jr, Colombari, D. S. & Menani, J. V. GABAergic mechanisms of the lateral parabrachial nucleus on sodium appetite. *Brain Res. Bull.* **73**, 238–247 (2007).
- De Gobbi, J. I. et al. Non-NMDA receptors in the lateral parabrachial nucleus modulate sodium appetite. *Brain Res.* **1301**, 44–51 (2009).
- Johnson, A. K. & Thunhorst, R. L. The neuroendocrinology of thirst and salt appetite: visceral sensory signals and mechanisms of central integration. *Front. Neuroendocrinol.* **18**, 292–353 (1997).
- Scalera, G., Spector, A. C. & Norgren, R. Excitotoxic lesions of the parabrachial nuclei prevent conditioned taste aversions and sodium appetite in rats. *Behav. Neurosci.* **109**, 997–1008 (1995).
- Geerling, J. C. et al. FoxP2 expression defines dorsolateral pontine neurons activated by sodium deprivation. *Brain Res.* **1375**, 19–27 (2011).
- Castro, L. et al. Central 5-HT_{2B/2C} and 5-HT₃ receptor stimulation decreases salt intake in sodium-depleted rats. *Brain Res.* **981**, 151–159 (2003).
- Gentili, L., Saija, A., Luchetti, G. & Massi, M. Effect of the 5-HT₂ antagonist ketanserin on salt appetite in the rat. *Pharmacol. Biochem. Behav.* **39**, 171–176 (1991).
- Menani, J. V., Thunhorst, R. L. & Johnson, A. K. Lateral parabrachial nucleus and serotonergic mechanisms in the control of salt appetite in rats. *Am. J. Physiol.* **270**, R162–R168 (1996).
- De Gobbi, J. I. et al. 5-HT₂ and 5-HT₃ receptors in the lateral parabrachial nucleus mediate opposite effects on sodium intake. *Neuroscience* **146**, 1453–1461 (2007).
- Yamamoto, T. et al. c-Fos expression in the parabrachial nucleus after ingestion of sodium chloride in the rat. *Neuroreport* **4**, 1223–1226 (1993).
- Geerling, J. C. & Loewy, A. D. Sodium deprivation and salt intake activate separate neuronal subpopulations in the nucleus of the solitary tract and the parabrachial complex. *J. Comp. Neurol.* **504**, 379–403 (2007).
- Ryan, P. J., Ross, S. I., Campos, C. A., Derkach, V. A. & Palmiter, R. D. Oxytocin-receptor-expressing neurons in the parabrachial nucleus regulate fluid intake. *Nat. Neurosci.* **20**, 1722–1733 (2017).
- Donnelly, M. L. et al. Analysis of the aphthovirus 2A/2B polyprotein ‘cleavage’ mechanism indicates not a proteolytic reaction, but a novel translational effect: a putative ribosomal ‘skip’. *J. Gen. Virol.* **82**, 1013–1025 (2001).
- Carter, M. E., Soden, M. E., Zweifel, L. S. & Palmiter, R. D. Genetic identification of a neural circuit that suppresses appetite. *Nature* **503**, 111–114 (2013).
- Campos, C. A. et al. Cancer-induced anorexia and malaise are mediated by CGRP neurons in the parabrachial nucleus. *Nat. Neurosci.* **20**, 934–942 (2017).
- Campos, C. A., Bowen, A. J., Schwartz, M. W. & Palmiter, R. D. Parabrachial CGRP neurons control meal termination. *Cell Metab.* **23**, 811–820 (2016).
- Garfield, A. S. et al. A neural basis for melanocortin-4 receptor-regulated appetite. *Nat. Neurosci.* **18**, 863–871 (2015).
- Stricker, E. M. & Verbalis, J. G. Central inhibitory control of sodium appetite in rats: correlation with pituitary oxytocin secretion. *Behav. Neurosci.* **101**, 560 (1987).
- Geerling, J. C., Chimenti, P. C. & Loewy, A. D. Phox2b expression in the aldosterone-sensitive HSD2 neurons of the NTS. *Brain Res.* **1226**, 82–88 (2008).
- Kang, B. J. et al. Central nervous system distribution of the transcription factor Phox2b in the adult rat. *J. Comp. Neurol.* **503**, 627–641 (2007).
- Hashimoto, K., Obata, K. & Ogawa, H. Characterization of parabrachial subnuclei in mice with regard to salt tastants: possible independence of taste relay from visceral processing. *Chem. Senses* **34**, 253–267 (2009).
- Biondillo, J. W., Williams, L. A. & King, M. S. Blocking glutamate receptors in the waist area of the parabrachial nucleus decreases taste reactivity behaviors in conscious rats. *Chem. Senses* **34**, 221–230 (2009).
- Chandrashekar, J. et al. The cells and peripheral representation of sodium taste in mice. *Nature* **464**, 297–301 (2010).
- Zardetto-Smith, A. M., Beltz, T. G. & Johnson, A. K. Role of the central nucleus of the amygdala and bed nucleus of the stria terminalis in experimentally-induced salt appetite. *Brain Res.* **645**, 123–134 (1994).
- Galaverna, O., De Luca, L. A. Jr, Schulkin, J., Yao, S. Z. & Epstein, A. N. Deficits in NaCl ingestion after damage to the central nucleus of the amygdala in the rat. *Brain Res. Bull.* **28**, 89–98 (1992).
- Dong, H. W., Petrovich, G. D. & Swanson, L. W. Topography of projections from amygdala to bed nuclei of the stria terminalis. *Brain Res. Rev.* **38**, 192–246 (2001).
- Dong, H. W., Petrovich, G. D., Watts, A. G. & Swanson, L. W. Basic organization of projections from the oval and fusiform nuclei of the bed nuclei of the stria terminalis in adult rat brain. *J. Comp. Neurol.* **436**, 430–455 (2001).
- Lee, S. et al. Chemosensory modulation of neural circuits for sodium appetite. *Nature* **568**, 93–97 (2019).
- Chen, Y., Baez, M. & Yu, L. Functional coupling of the 5-HT_{2C} serotonin receptor to G proteins in *Xenopus* oocytes. *Neurosci. Lett.* **179**, 100–102 (1994).
- Lucaites, V. L., Nelson, D. L., Wainscott, D. B. & Baez, M. Receptor subtype and density determine the coupling repertoire of the 5-HT₂ receptor subfamily. *Life Sci.* **59**, 1081–1095 (1996).
- Kurachi, Y., Tung, R. T., Ito, H. & Nakajima, T. G protein activation of cardiac muscarinic K⁺ channels. *Prog. Neurobiol.* **39**, 229–246 (1992).
- Petrov, T., Krukoff, T. L. & Jhamandas, J. H. The hypothalamic paraventricular and lateral parabrachial nuclei receive collaterals from raphe nucleus neurons: a combined double retrograde and immunocytochemical study. *J. Comp. Neurol.* **318**, 18–26 (1992).
- Bang, S. J., Jensen, P., Dymecki, S. M. & Commons, K. G. Projections and interconnections of genetically defined serotonin neurons in mice. *Eur. J. Neurosci.* **35**, 85–96 (2012).
- Smits, J. F., van Essen, H. & Struyker-Boudier, H. A. Serotonin-mediated cardiovascular responses to electrical stimulation of the raphe nuclei in the rat. *Life Sci.* **23**, 173–178 (1978).

Publisher's note Springer Nature remains neutral with regard to jurisdictional claims in published maps and institutional affiliations.

© The Author(s), under exclusive licence to Springer Nature America, Inc. 2020

Methods

Animals. Htr2c-2A-iCre mice were generated by conventional gene targeting in C57BL/6 embryonic stem cells. All resulting chimeras displaying germline transmission were bred to mice of C57BL/6 background. The F₁ pups from male chimeras were screened for those carrying the *Htr2c^{iCre}* allele using PCR genotyping with the following primers: CL-9631: 5'-TTTGTGGGAAGGCCTGTAAC-3'; CL-10057: 5'-GGAGTGGGGACTT TCCTAC-3'; CL-R309: 5'-TCCCTCACATCCTCAGGTTC-3'. *Htr2c^{fl/w/y}* mice were described previously⁴⁰. Htr2c-2A-iCre mice were crossed with tdTomato (Ai14) reporter mice, Gt(Rosa)26Sortm14(CAG-tdTomato)Hze/J, for patch-clamp recordings. Mice were housed at 22–24°C with a 12-h light/12-h dark cycle on normal chow (Teklad, 2018S). Sodium-deficient diet (D08070603, Research Diets) and control diet (TD94045; Teklad) were given only during experimental procedures. Food and water were provided ad libitum when experiments were not being conducted. Six- to eight-week-old male mice were used for surgery. Allocation of animals to control or experimental groups was randomized and counterbalanced. The investigator was not blinded to group allocation. The investigator was not blinded to experimental or control groups during behavioral experiments. However, all behavioral experiments involved stereotaxic injections, thus blinding the investigator to whether the mice passed or failed viral expression inclusion criteria. All procedures were conducted according to the Korean Advanced Institute of Science and Technology (KAIST) Guidelines for the Care and Use of Laboratory Animals and were approved by the Institutional Animal Care and Use Committee (protocol no. KA2018-80).

Stereotaxic injections. Mice were anesthetized under isoflurane and had their heads fixed in a stereotaxic frame. Lidocaine (2% wt/vol) was applied topically for preemptive analgesia. The skull was drilled and a 33-gauge blunt NanoFil needle (NF33BL-2, World Precision Instruments) was lowered to the target region (LPBN: A–P, 5.22 mm; M–L, 1.3 mm; D–V, 3.5 mm) toward the target nucleus. For chemogenetic experiments, 0.08–0.15 μ l of AAV5-hSyn-DIO-hM3q-mCherry virus (3.8×10^{12} molecules per μ l; University of North Carolina Vector Core), AAV2-hSyn-DIO-hM4Di-mCherry (3.7×10^{12} molecules per μ l; University of North Carolina Vector Core) or AAV2-hSyn-DIO-mCherry (5.6×10^{12} molecules per μ l; University of North Carolina Vector Core) was injected into the LPBN of Htr2c-2A-iCre mice using a Hamilton syringe at a rate of 0.2 μ l min⁻¹. Then, 7–10 min after injection of the virus, the needle was slowly removed. For optogenetic experiments, 0.12–0.14 μ l of AAV5-EF1a-DIO-hChR2 (E123T/T159C)-p2A-EYFP (5.1×10^{12} molecules per μ l; University of North Carolina Vector Core), AAV5-EF1a-DIO-EYFP (6.5×10^{12} molecules per μ l; University of North Carolina Vector Core), AAV2-EF1a-DIO-hChR2 (H134R)-p2A-mCherry (5.1×10^{12} molecules per μ l; University of North Carolina Vector Core) or AAV2-EF1a-DIO-mCherry (3.2×10^{12} molecules per μ l; University of North Carolina Vector Core) was injected. Monofiber optic cannulas (200- μ m-diameter core; NA = 0.37) were implanted at A–P, 5.22 mm; M–L, 1.3 mm; and D–V, 3.2 mm for LPBN soma photostimulation and A–P, 1.22; M–L, 2.5; and D–V 4.1 mm for CeA terminal photostimulation, with Super-Bond C&B (Sun Medical). For conditional *Htr2c* deletion experiments, AAV5-CMV-GFP (4.7×10^{12} molecules per μ l; University of North Carolina Vector Core) or AAV5-CMV-Cre-GFP (4.5×10^{12} molecules per μ l; University of North Carolina Vector Core) was injected into the LPBN of Htr2c^{fl/w/y} mice. Mice were kept on a heating pad and watched closely until regaining movement. Mice were handled for 1 week before starting behavioral experiments. At least 3 weeks of recovery were given before starting behavioral experiments. For anterograde tracing experiments, 0.1–0.16 μ l of AAV5-EF1a-DIO-EYFP (6.5×10^{12} molecules per μ l; University of North Carolina Vector Core) was injected into the LPBN of Htr2c-2A-iCre mice. Mice were killed 3 weeks later. For retrograde tracing, 0.12–0.17 μ l of red retrobeads (Lumafuor) was injected into the LPBN of Htr2c-2A-iCre mice. Mice were killed 5 d later.

Immunohistochemistry. Mice were anesthetized with isoflurane and transcardially perfused with saline, followed by 4% paraformaldehyde (PFA), and had their brains extracted. Brains were fixed overnight in PFA at 4°C. After fixation, brains were cryoprotected in a 30% sucrose solution at 4°C for 1–2 d. Brains were then frozen in FSC Clear (Leica) and sliced using a cryotome (Leica, CM1850) at 30- μ m thickness. Slices were incubated in a blocking solution (2% goat serum and 0.3% Triton X-100, in 0.1 M PBS) for 1 h at room temperature on a shaking plate. Slices were then incubated in primary antibodies—1:1,000 rabbit anti-CGRP (T4032, Bachem) or 1:1,000 rabbit anti-serotonin (20080, Immunostar) solution—for 17 h at 4°C. Slices were then washed for 10 min, three times in PBS. Slices were incubated in a secondary antibody solution for 1 h. A secondary antibody—goat anti-rabbit 647 (A21245, Molecular Probes)—was used at 1:200 dilution. Slices were washed for 10 min three times in PBS. DAPI was added (1:10,000) during the second PBS wash. Slices were then mounted on a microscope glass with DAKO mounting medium. z-stack images were acquired with a confocal microscope (LSM780, Zeiss), and maximum-intensity z was projected with ImageJ (NIH) software.

Fluorescence in situ hybridization. Mice were anesthetized with isoflurane, transcardially perfused with DEPC-PBS, followed by 4% PFA, and had their brains

extracted. Brains were fixed overnight in PFA at 4°C. After fixation, brains were cryoprotected in a 30% sucrose solution at 4°C for 1–2 d. Brains were then frozen in O.C.T. compound (4583, Tissue-Tek) and sliced using a cryotome (CM1850, Leica) at 14- μ m thickness at the KAIST Bio-core center. Slices were stored in a cryoprotectant solution (500 ml 0.1 M phosphate buffer (pH 7.2), 300 ml ethylene glycol and 300 g sucrose, with the remaining volume filled with distilled water to a total of 1 l) at –20°C until further processing. mRNA signals were hybridized using RNAscope, according to the manufacturer's instructions. Protease treatment was done for 15 min at 40°C using the HybEZ Hybridization System. Mm-Htr1b (315861), Mm-Foxp2 (428791), Mm-Oxtr (412171), Mm-Fos-C2 (316921-C2) and Mm-Htr2c-C3 (401001-C3) were used to detect *Htr1b*, *Foxp2*, *Oxtr*, *Fos* and *Htr2c* mRNA, respectively. For *Fos* experiments, wild-type mice were acclimated to oral gavages by intragastrically loading them with saline for 1 week (10 μ g l⁻¹). On the day of the assay, normal saline (154 mM NaCl) or hypertonic saline (1.5 M NaCl) was gastrically loaded into animals at 10 μ g l⁻¹. Animals were killed 25 min later. For conditional knockout experiments, EGFP-C1 (400281) and a custom-made Mm-Htr2c-01-C3 probe (503281) that recognizes base pairs 724–1,241 of NM_008312.4 were used to visualize *GFP* and *Htr2c* mRNA, respectively. z-stack images were acquired with a confocal microscope (LSM780, Zeiss), and maximum-intensity z was projected with ImageJ (NIH) software.

Behavioral experiments. For fast-refeeding experiments, mice were housed in single cages for at least 1 week before conducting assays. The day before the assay, mouse body weights were measured, food was cleared and bedding was replaced. Stock CNO was dissolved in DPBS at 8.75 mM. Stock CNO was diluted in sterile saline and administered intraperitoneally at 1 mg kg⁻¹, while DPBS was administered by diluting in sterile saline at a ratio consistent with CNO injections. In the text, saline injections refer to DPBS diluted in sterile saline. Injections were given 18 h after fasting, at 10:00 on the day of the assay. Food was then reintroduced (normal chow, sodium-deficient diet or control diet), and food intake and body weight were measured at 1, 2 and 4 h after intraperitoneal injections. For two-bottle assays, mice were housed in single cages equipped with two volumetric drinking tubes (MedAssociates) containing either distilled water or 300 mM NaCl for at least 1 week before conducting assays. For sodium depletion, furosemide was administered subcutaneously at 50 mg kg⁻¹ at 19:30 on the day before the assay. After furosemide injections, chow diet was replaced with a sodium-deficient diet (D08070603, Research Diets), bedding was replaced and 300 mM NaCl bottles were removed. At 18:45 on the day of the assay, mice were injected with either saline or CNO in a counterbalanced, randomized manner. Water and sodium-deficient diet were then removed. Assays began at 19:30, upon the reintroduction of distilled water and 300 mM NaCl solution. For one-bottle assays, mice were acclimated to a lickometer-installed cage before testing. Mice were trained to use the lickometer-connected sipper bottle by depriving them of water and introducing them into the lickometer-installed cage the next day. Training was considered successful when mice made at least 100 licks within 30 min. On the day before testing, sodium depletion was carried out using the same sodium depletion protocol for two-bottle assays. On the day of testing, mice were first habituated in the testing cage for 15 min without food, water or 300 mM NaCl. A bottle containing 300 mM NaCl was then introduced, and the number of licks was measured for 20 min. No-photostimulation and photostimulation conditions were conducted at the same time of day for each mouse. All one-bottle assays were conducted during the dark cycle. For dehydration, both distilled water and 300 mM NaCl bottles were removed at 23:30 on the day before the assay. At 18:45 on the day of the assay, mice were injected with either saline or CNO in a counterbalanced, randomized manner. Normal chow was removed and bedding was replaced. Assays began at 19:30, upon the reintroduction of distilled water and 300 mM NaCl solution.

For evolesmic experiments, distilled water, 300 mM salt solution and normal chow were available ad libitum until saline and CNO injections, at 18:45 on the day of the assay. Distilled water, 300 mM salt solution and normal chow were then removed and the bedding was replaced. Assays began at 19:30, upon the reintroduction of distilled water and 300 mM salt solution. All chemogenetic experiments were done as paired comparisons in which assays were repeated at least 4 d later, with the treatments switched (that is, saline to CNO or CNO to saline). Experiments with knockout mice were conducted using littermates. The investigator was not blinded to whether mice belonged to experimental or control groups.

Photostimulation protocol. Patch cords (1 m long, 200- μ m core diameter; Doric Lenses) were connected from a rotary joint (Doric Lenses) to monofiber optic cannulas through zirconia sleeves (Doric Lenses). A custom-made lickometer (Arduino) was used to detect licks and drive photostimulation upon each lick (10 Hz, 10-ms pulse width, 1-s duration). Blue light was generated from a laser (473 nm; Laserglow) at an intensity of 8.2–11.3 mW as measured at the tip of the optic cannula. We estimated the light power at the LPBN to be approximately 9.2–12.67 mW mm⁻² and at the CeA to be 14.4–21 mW mm⁻² as calculated by an online light transmission calculator (<http://web.stanford.edu/group/dlab/cgi-bin/graph/chart.php>).

Histology. After completion of behavioral experiments, mice were perfused with saline and 4% PFA. Brains were extracted and post fixed for 24 h at 4°C in 4% PFA.

Then 50- μm sections were made on a vibratome (VT1200S; Leica) and mounted with Vectashield Mounting Medium with DAPI, Hard Set (H-1500, Vector). Mice were excluded from analysis if vector expression was absent, incomplete or outside the area of interest. For optogenetic experiments, optic fiber tip locations were also validated and excluded when off target.

Electrophysiology. Whole-cell patch-clamp recordings from Htr2c neurons were made from the LPBN of 3- to 6-week-old male and female mice. Mice were anesthetized with isoflurane and transcardially perfused with a cutting solution (220 mM sucrose, 26 mM NaHCO_3 , 2.5 mM KCl, 1 mM NaH_2PO_4 , 5 mM MgCl_2 , 1 mM CaCl_2 , 10 mM glucose; pH 7.3–7.35). The mice were then decapitated, and the entire brain was removed and immediately submerged in ice-cold carbogen-saturated cutting solution. Then, 300- μm coronal sections were cut from the LPBN with a Leica VT1200S vibratome and incubated in oxygenated storage solution (123 mM NaCl, 26 mM NaHCO_3 , 2.8 mM KCl, 1.25 mM NaH_2PO_4 , 1.2 mM MgSO_4 , 2.5 mM CaCl_2 , 10 mM glucose; pH 7.3–7.35) at 34°C for at least 1 h before recording. Slices were transferred to the recording chamber and allowed to equilibrate for 10 min before recording. Recordings were made in the presence of a recording solution (126 mM NaCl, 26 mM NaHCO_3 , 2.8 mM KCl, 1.25 mM NaH_2PO_4 , 1.2 mM MgSO_4 , 2.5 mM CaCl_2 , 5 mM glucose; pH 7.3–7.35). The pipette solution for current-clamp, whole-cell recording was modified to include an intracellular dye (Alexa Fluor 488: 120 mM potassium gluconate, 10 mM KCl, 10 mM HEPES, 5 mM EGTA, 1 mM CaCl_2 , 1 mM MgCl_2 , 2 mM MgATP; pH 7.29). Epifluorescence was briefly used to target fluorescent cells, at which time the light source was switched to infrared differential interference contrast imaging to obtain the whole-cell recording (Nikon Eclipse FN-S2N equipped with a fixed stage and a QImaging optiMOS sCMOS camera). Electrophysiological signals were recorded using an Axopatch 700B amplifier (Molecular Devices), low-pass filtered at 2–5 kHz and analyzed offline on a PC with Clampfit (Molecular Devices). Recording electrodes had resistances of 2–6 M Ω when filled with the potassium gluconate internal solutions. Input resistance was assessed by measuring voltage deflection at the end of the response to hyperpolarizing rectangular current pulse steps (500 ms, from -5 to -25 pA, -10 to -50 pA or -20 to -100 pA). Membrane potential values were not compensated to account for junction potential (-8 mV). Cell-attached recordings were made either from 4- to 6-week-old Htr2c-2A-iCre::tdTomato mice or 7-week-old Htr2c-2A-iCre mice injected with AAV-DIO-EYFP. Recordings were carried out by filling pipettes with recording solution and at a holding potential of 0 mV. Photostimulation was delivered through an Optopatcher (A-M Systems), connected to a laser source (473 nm; Laserglow), through a patch cord with an NA of 4.8. Light intensity at the end of the optic fiber was measured as 6–8.4 mW. CRACM experiments were conducted in voltage-clamp mode at -60 mV and -10 mV to detect excitatory and inhibitory postsynaptic currents, respectively. Three single light pulses (10 ms) were delivered 1 s apart by triggering a pulse generator with pClamp software.

Drugs. TTX, picrotoxin, kynurenic acid, SB216641 and mCPP were acquired from Tocris. Lidocaine, tolbutamide and CNO were acquired from Sigma. Stock solutions of tolbutamide were made by dissolving in ethanol. Stock solutions of TTX, picrotoxin, kynurenic acid and SB216641 were made by dissolving in distilled water. Stock solutions of CNO and mCPP were made in DPBS (D8537, Sigma).

Statistics. All statistics were done using Prism v6.01 (GraphPad) software. For electrophysiology experiments, nonparametric statistical tests (two-tailed Wilcoxon signed-rank test or Mann–Whitney test) or repeated-measures ANOVA with a Greenhouse–Geisser correction was used. For electrophysiology experiments, n represents the final number of recorded cells. All chemogenetic experiments were analyzed using two-way repeated-measures ANOVA matched by time and treatment. Optogenetic experiments were analyzed using two-way repeated-measures ANOVA matched by photostimulation conditions. For

fluorescence in situ hybridization, data were analyzed using two-tailed Mann–Whitney or two-way ANOVA tests. Htr2c^{lox/y} experiments were analyzed using two-way repeated measures ANOVA matched across time. Post hoc comparisons were always done using the Bonferroni correction. Adjusted P values for post hoc comparisons are presented in Supplementary Table 1. n represents the final number of validated healthy animals. Data distribution was assumed to be normal, but this was not formally tested. Sample sizes were not predetermined but were matched to those in similar literature^{19,22}.

Reporting Summary. Further information on research design is available in the Nature Research Reporting Summary linked to this article.

Data availability

The data that support the findings of this study are available from the corresponding authors upon reasonable request.

Code availability

Custom code used in this study is available from the corresponding authors upon reasonable request.

References

- Berglund, E. D. et al. Serotonin 2C receptors in pro-opiomelanocortin neurons regulate energy and glucose homeostasis. *J. Clin. Invest.* **123**, 5061–5070 (2013).

Acknowledgements

We thank G.S.B. Suh (KAIST) for helpful comments on the manuscript, S.-H. Lee (KAIST) for technical help with viral tracing experiments and D. Kim (KAIST) for technical help with imaging. This work was supported by grants from the Samsung Science & Technology Foundation (SSTF-BA1901-11 to J.-W.S.), the KAIST Future Systems Health Care Project (to J.-W.S.), the KAIST Venture Research Program for Graduate and PhD students (to S.P.), the American Heart Association (16SDG27260001 to C.L.) and the National Institutes of Health (R01 DK114036 to C.L. and R01 DK100699, R01 DK119169, DK119130 5830 to K.W.W.). S.P. was supported in part by stipends from the National Research Foundation of Korea (NRF-2015M3A9E7029177 and NRF-2016R1C1B2006614 to J.-W.S.).

Author contributions

S.P. and J.-W.S. designed the experiments. S.P. conducted experiments and analyzed data. C.L. and K.W.W. provided reagents and expertise. C.L. generated and validated Htr2c-2A-iCre mice. S.P. and J.-W.S. wrote the manuscript. All authors discussed the results and commented on the manuscript.

Competing interests

The authors declare no competing interests.

Additional information

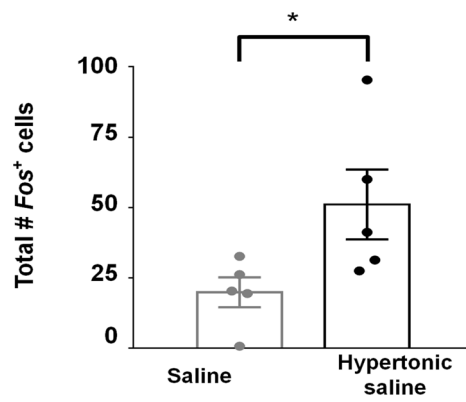
Extended data is available for this paper at <https://doi.org/10.1038/s41593-019-0573-2>.

Supplementary information is available for this paper at <https://doi.org/10.1038/s41593-019-0573-2>.

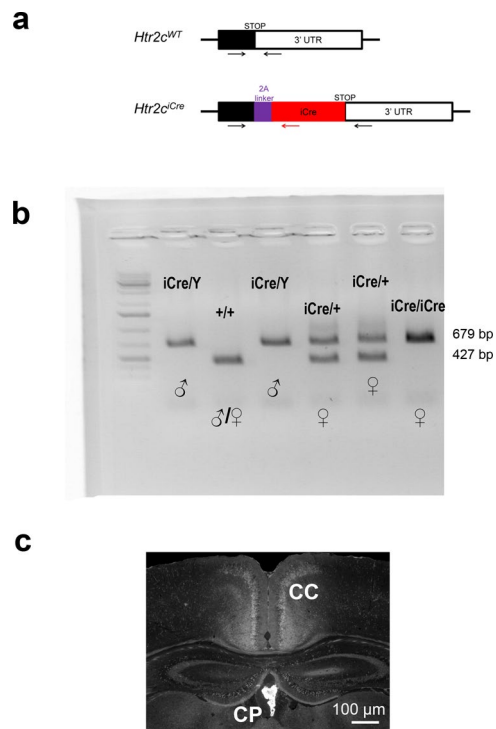
Correspondence and requests for materials should be addressed to C.L. or J.-W.S.

Peer review information *Nature Neuroscience* thanks Yuki Oka and the other, anonymous, reviewer(s) for their contribution to the peer review of this work.

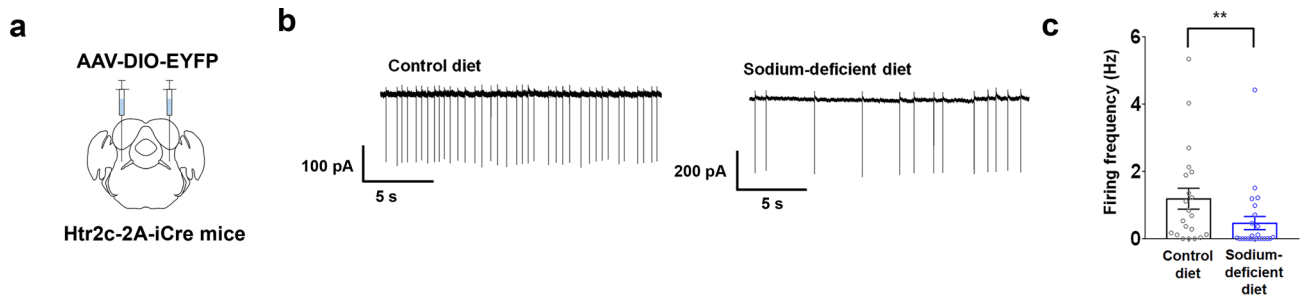
Reprints and permissions information is available at www.nature.com/reprints.



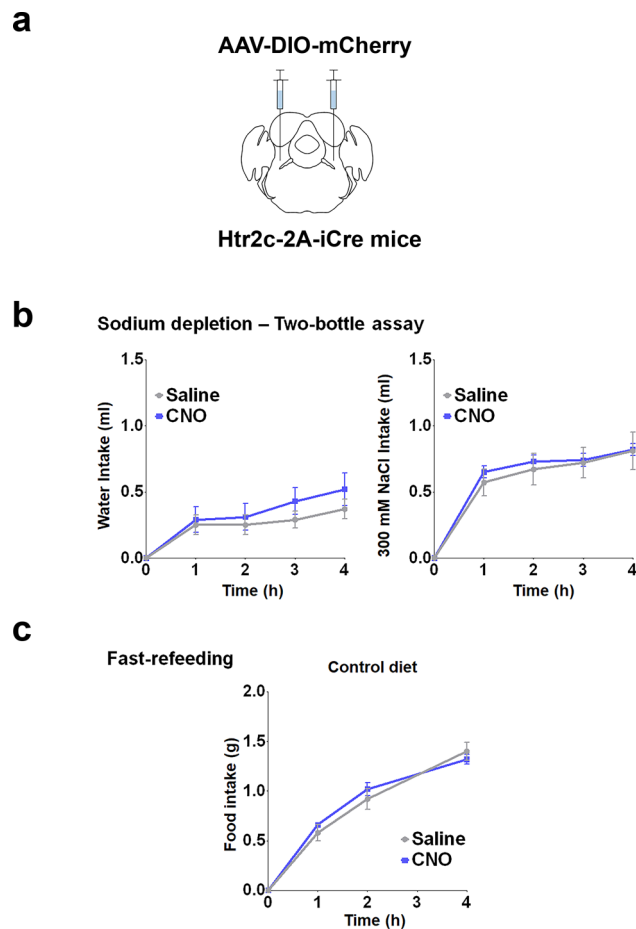
Extended Data Fig. 1 | LPBN neurons respond to hypertonic saline. Hypertonic saline-loaded mice show more *Fos* in the LPBN than saline-loaded controls. Two-tailed Mann-Whitney test, Saline N = 5 mice, Hypertonic saline N = 5 mice. P = 0.0317. All data represented as mean \pm s.e.m. *P < 0.05.



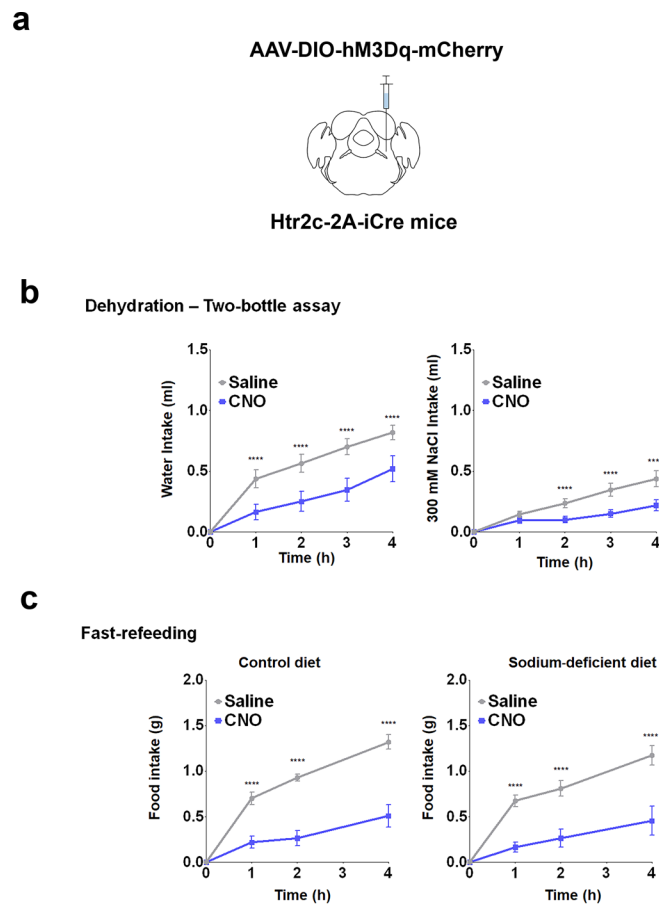
Extended Data Fig. 2 | Generation of an Htr2c-2A-iCre mouse line. (a) Htr2c-2A-iCre knock-in mice in which the coding sequences of *Htr2c* and *iCre* are linked by a viral peptide bridge 2A sequence. **(b)** Detection of wildtype and targeted *Htr2c* alleles by PCR genotyping. Similar results were obtained with at least 3 independent replications. **(c)** Immunohistochemical analysis of Htr2c-2A-iCre activity using a tdTomato reporter. Note high levels of tdTomato expression in the choroid plexus (CP). CC = corpus callosum. Similar results were obtained with at least 3 mice. Scale bar = 100 μ m Source data.



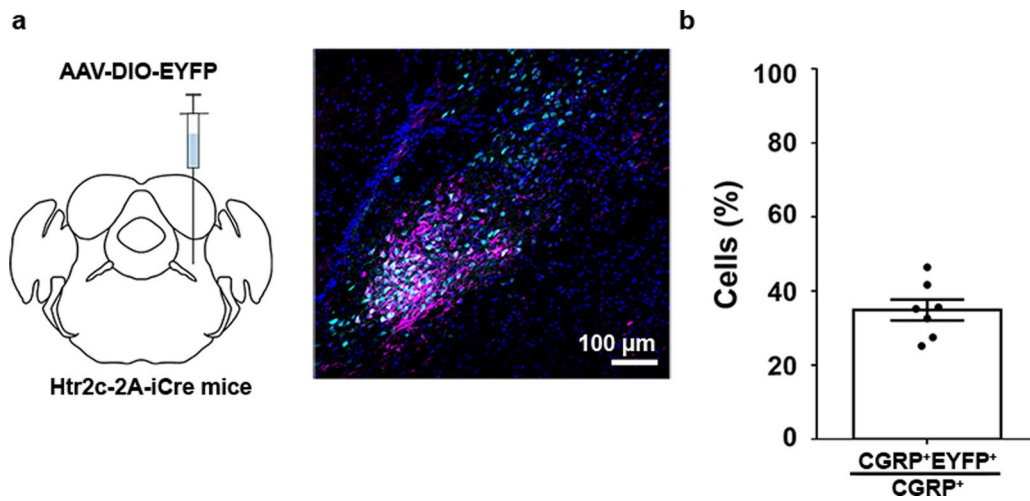
Extended Data Fig. 3 | EYFP-expressing LPBN^{Htr2c} neurons are inhibited during sodium depletion. (a) Cell-attached recordings taken from Htr2c-2A-iCre mice injected with AAV5-E1fa-DIO-EYFP. (b) Representative cell-attached recording of LPBN^{Htr2c} neurons after 7 days of control diet, or 7 days of sodium-deficient diet. (c) Firing frequency of LPBN^{Htr2c} neurons between control diet-fed mice (left) and sodium-deficient diet-fed mice (right). Two-tailed Mann-Whitney test. Control diet $n = 21$ cells, sodium-deficient diet $n = 24$ cells. Control diet 1.2 ± 0.3 Hz, Sodium-deficient diet 0.4 ± 0.2 Hz, $P = 0.007$. All data represented as mean \pm s.e.m. ****** $P < 0.01$.



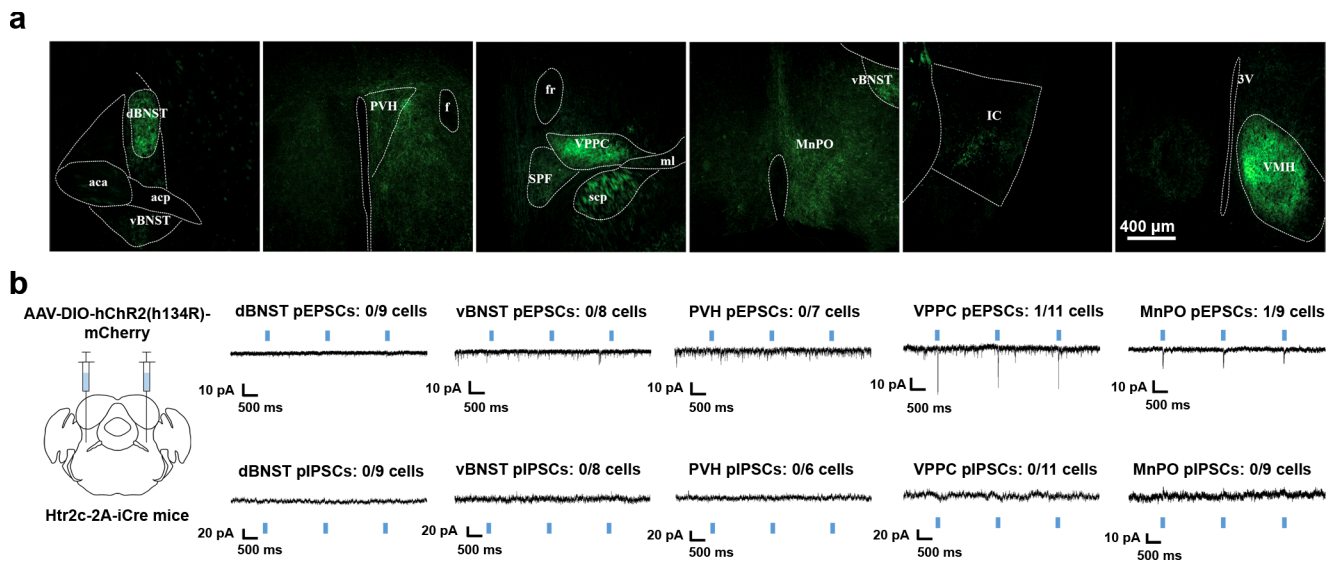
Extended Data Fig. 4 | CNO injections in AAV-DIO-mCherry-injected controls do not affect food intake, water intake or 300 mM NaCl intake. (a) Htr2c-2A-iCre mice injected with AAV2-hSyn-DIO-mCherry showed no changes in food intake, body weight or 300 mM NaCl intake. **(b)** No changes in water intake or 300 mM NaCl intake during sodium depletion. $N = 5$ mice. Water intake during sodium depletion: Two-Way Repeated Measures ANOVA: time ($F(4, 16) = 20.52, P < 0.0001$), treatment ($F(1, 4) = 0.5421, P = 0.5024$), interaction ($F(4, 16) = 0.6448, P = 0.6385$). 300 mM NaCl intake during sodium depletion: Two-Way Repeated Measures ANOVA: time ($F(4, 16) = 108.1, P < 0.0001$), treatment ($F(1, 4) = 0.1128, P = 0.7538$), interaction ($F(4, 16) = 0.3142, P = 0.8643$). **(c)** No changes in food intake or body weight when using a control diet. $N = 5$ mice. Control diet food intake: Two-Way Repeated Measures ANOVA: time ($F(3, 12) = 223.9, P < 0.0001$), treatment ($F(1, 4) = 0.2222, P = 0.6619$), interaction ($F(3, 12) = 2.689, P = 0.0924$). All data represented as mean \pm s.e.m.



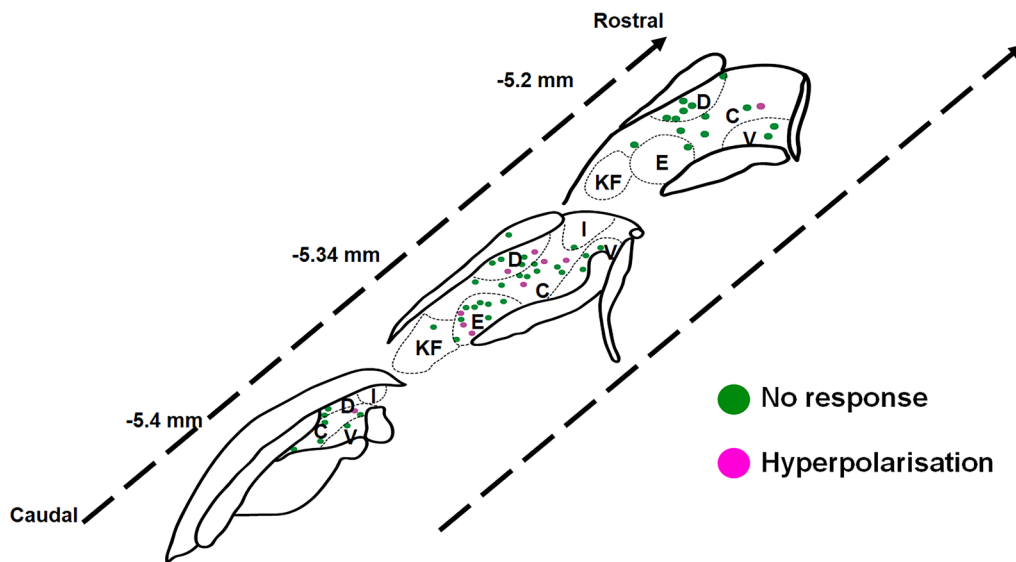
Extended Data Fig. 5 | LPBN^{Htr2c} neuron activation can cause non-sodium related effects. (a) Unilateral injection of AAV5-hSyn-DIO-hM3Dq into the LPBN of Htr2c-2A-iCre mice. (b) Activation of LPBN^{Htr2c} neurons decreased water and 300 mM NaCl intake during dehydration in a two-bottle choice assay. N = 11. Water intake during dehydration: Two-Way Repeated Measures ANOVA: time ($F(4,40) = 67.06$, $P < 0.0001$), treatment ($F(1, 10) = 8.707$, $P = 0.0145$), interaction ($F(4, 40) = 6.329$, $P = 0.0005$). Post hoc tests using the Bonferroni correction. 300 mM NaCl intake during dehydration: Two-Way Repeated Measures ANOVA: time ($F(4,40) = 31.38$, $P < 0.0001$), treatment ($F(1, 10) = 17.76$, $P = 0.0018$), interaction ($F(4, 40) = 14.06$, $P = 0.0001$). (c) Activation of LPBN^{Htr2c} neurons decreased food during a fast refeeding regardless of sodium content. N = 11. Control diet food intake (left): Two-Way Repeated Measures ANOVA: time ($F(3,30) = 111.0$, $P < 0.0001$), treatment ($F(1, 10) = 51.2$, $P < 0.0001$), interaction ($F(3, 30) = 32.00$, $P < 0.0001$). Sodium-deficient diet food intake (right): Two-Way Repeated Measures ANOVA: time ($F(3,30) = 50.59$, $P < 0.0001$), treatment ($F(1, 10) = 27.74$, $P = 0.0004$), interaction ($F(3, 30) = 18.81$, $P < 0.0001$). All *post hoc* tests using the Bonferroni correction. All data represented as mean \pm s.e.m. **** $P < 0.0001$.



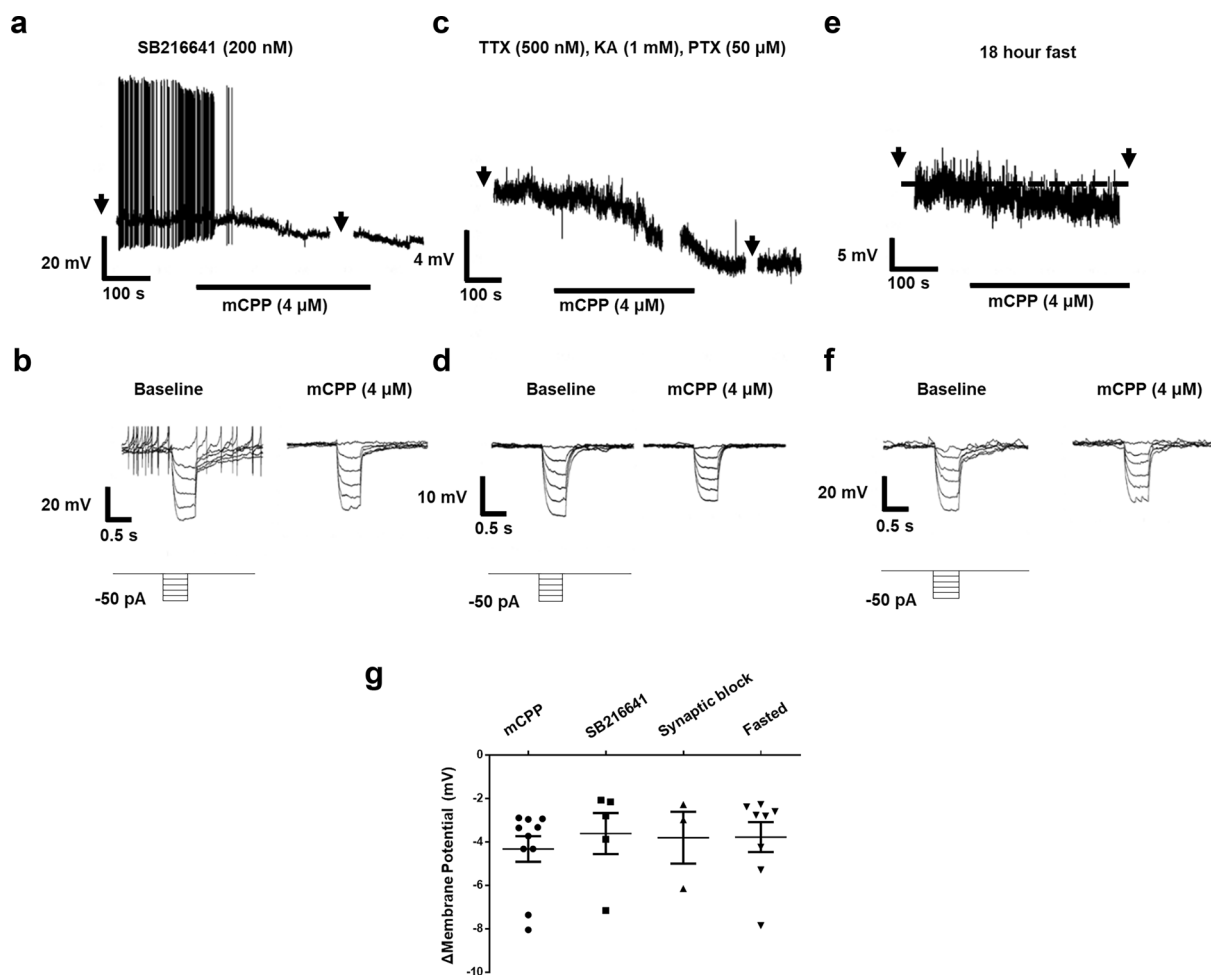
Extended Data Fig. 6 | LPBN^{Htr2c} neurons colocalise with CGRP. (a) Schematic of experiment. Unilateral injection of AAV5-EF1a-DIO-EYFP into the LPBN of Htr2c-2A-iCre mice to visualise LPBN^{Htr2c} neurons (left). Colocalisation of EYFP labelled LPBN^{Htr2c} neurons with CGRP (right). Cyan = EYFP, Magenta = CGRP, Blue = DAPI. Scale bar = 100 μ m. (b) Estimation of colocalisation between LPBN^{Htr2c} neurons and CGRP neurons. 3 slices taken from each mice. N = 7 mice.



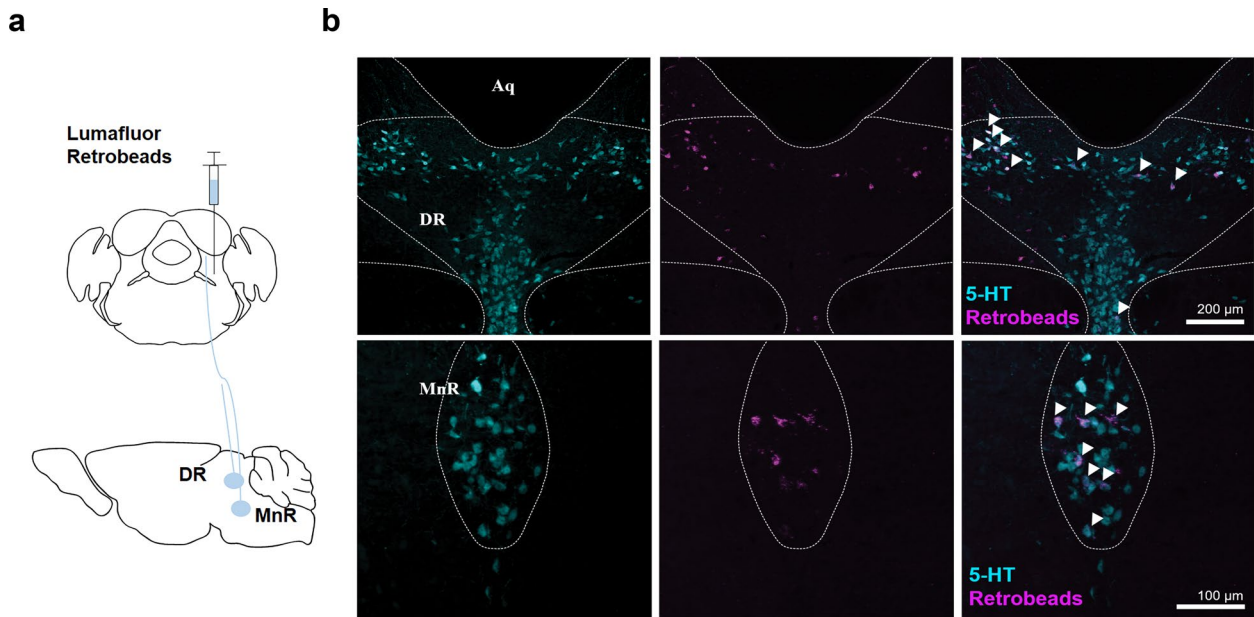
Extended Data Fig. 7 | Downstream circuitry of LPBN^{Htr2c} neurons. (a) Axonal projections visualised by unilateral injection of AAV5-EF1a-DIO-EYFP into the LPBN of Htr2c-2A-iCre mice. aca = anterior commissure (anterior part), acp = anterior commissure (posterior part), dBNST = bed nucleus of the stria terminalis (lateral division), fr = fasciculus retroflexus, ml = medial lemniscus, MnPO = median preoptic nucleus, opt = optic tract, PVH = paraventricular nucleus of the hypothalamus, scp = superior cerebellar peduncle, SPF = subparafascicular thalamus, st = stria terminalis, vBNST = bed nucleus of the stria terminalis (ventral part), VPPC = ventral posterior thalamus (parvicellular part). Scale bar = 400 μ m. N = 7 mice. **(b)** Schematic of experiment. Bilateral injection of AAV2-DIO-hChR2 (H134R)-p2A-mCherry into the LPBN of Htr2c-2A-iCre mice (left). Voltage-clamp recordings taken at downstream sites (traces on the right). Blue rectangles indicate times of photostimulation.



Extended Data Fig. 8 | Illustration showing the approximate spatial distribution of mCPP-responsive neurons within the LPBN. C = central LPBN, D = dorsal LPBN, E = external LPBN, I = internal LPBN, KF = Kolliker's Fuse, V = ventral LPBN.



Extended Data Fig. 9 | Hyperpolarisation of LPBN^{Htr2c} neurons is not dependent on Htr1b and is postsynaptic. (a) Representative current clamp recording of an LPBN^{Htr2c} neuron pre-treated with SB216641 (200 nM). Hyperpolarisation in response to mCPP persists in presence of SB216641. Arrows indicate time at which current steps were applied. (b) Voltage deflections in response to hyperpolarising currents from the same neuron, showing decreased input resistance in response to mCPP. Current steps in trace made in 10 pA increments from -50 pA to 0 pA. (c) Representative current clamp recording of an LPBN^{Htr2c} neuron pre-treated with TTX (500 nM), kynurenic acid (KA, 1 mM) and picrotoxin (PTX, 50 μM), showing hyperpolarisation in response to mCPP. Arrows indicate time at which current steps were applied. (d) Voltage deflections in response to hyperpolarising currents from the same neuron, showing decreased input resistance in response to mCPP. Current steps in trace made in 10 pA increments from -50 pA to 0 pA. (e) Representative current clamp recording of an LPBN^{Htr2c} neuron from a fasted mouse (18 hours), showing hyperpolarisation in response to mCPP. Arrows indicate time at which current steps were applied. (f) Voltage deflections in response to hyperpolarising currents from the same neuron, showing decreased input resistance in response to mCPP. Current steps in trace made in 10 pA increments from -50 pA to 0 pA. (g) Graph summarising change in membrane potential in response to mCPP under conditions tested. Neither pre-treatment with SB216641, Synaptic blockers nor recordings from fasted mice changed the magnitude of response to mCPP. mCPP n = 10 cells, SB216641 n = 5 cells, Synaptic block n = 3 cells, Fasted n = 8 cells. Data represented as mean ± s.e.m.



Extended Data Fig. 10 | Serotonergic projections to the LPBN. (a) Schematic of experiment. Unilateral injection of Lumafluor retrobeads into the LPBN of wildtype mice to visualise upstream neurons. **(b)** Arrows indicate colocalised cells. Aq = aqueduct, DR = dorsal raphe. Scale bar = 200 μ m. N = 6 mice (upper). MnR = median raphe. Scale bar = 100 μ m. N = 6 mice (lower).

Reporting Summary

Nature Research wishes to improve the reproducibility of the work that we publish. This form provides structure for consistency and transparency in reporting. For further information on Nature Research policies, see [Authors & Referees](#) and the [Editorial Policy Checklist](#).

Statistics

For all statistical analyses, confirm that the following items are present in the figure legend, table legend, main text, or Methods section.

n/a Confirmed

- The exact sample size (n) for each experimental group/condition, given as a discrete number and unit of measurement
- A statement on whether measurements were taken from distinct samples or whether the same sample was measured repeatedly
- The statistical test(s) used AND whether they are one- or two-sided
Only common tests should be described solely by name; describe more complex techniques in the Methods section.
- A description of all covariates tested
- A description of any assumptions or corrections, such as tests of normality and adjustment for multiple comparisons
- A full description of the statistical parameters including central tendency (e.g. means) or other basic estimates (e.g. regression coefficient) AND variation (e.g. standard deviation) or associated estimates of uncertainty (e.g. confidence intervals)
- For null hypothesis testing, the test statistic (e.g. F , t , r) with confidence intervals, effect sizes, degrees of freedom and P value noted
Give P values as exact values whenever suitable.
- For Bayesian analysis, information on the choice of priors and Markov chain Monte Carlo settings
- For hierarchical and complex designs, identification of the appropriate level for tests and full reporting of outcomes
- Estimates of effect sizes (e.g. Cohen's d , Pearson's r), indicating how they were calculated

Our web collection on [statistics for biologists](#) contains articles on many of the points above.

Software and code

Policy information about [availability of computer code](#)

Data collection

Electrophysiology data were collected using Clampex (Molecular Devices) Version 10.5.1.0. Confocal images were obtained with Zeiss Imaging Software (From LSM 780).

Data analysis

All statistics were done using Prism (GraphPad) software Version 6.01.
Electrophysiology data was analysed using Clampfit (Molecular Devices) Version 10.4.0.36.
Figures for electrophysiology data were prepared using Igor Pro (WaveMetrics, Inc) Version 4.0.1.0.
Confocal data were analysed using ZEN2009 Light Edition.
Image data were prepared using ImageJ (NIH) Version 1.48.

For manuscripts utilizing custom algorithms or software that are central to the research but not yet described in published literature, software must be made available to editors/reviewers. We strongly encourage code deposition in a community repository (e.g. GitHub). See the Nature Research [guidelines for submitting code & software](#) for further information.

Data

Policy information about [availability of data](#)

All manuscripts must include a [data availability statement](#). This statement should provide the following information, where applicable:

- Accession codes, unique identifiers, or web links for publicly available datasets
- A list of figures that have associated raw data
- A description of any restrictions on data availability

The data that support the findings of this study are available from the corresponding author upon reasonable request.

Field-specific reporting

Please select the one below that is the best fit for your research. If you are not sure, read the appropriate sections before making your selection.

Life sciences Behavioural & social sciences Ecological, evolutionary & environmental sciences

For a reference copy of the document with all sections, see [nature.com/documents/nr-reporting-summary-flat.pdf](https://www.nature.com/documents/nr-reporting-summary-flat.pdf)

Life sciences study design

All studies must disclose on these points even when the disclosure is negative.

Sample size	Sample sizes were not predetermined, but matched to similar literatures. (Carter, M. E., Soden, M. E., Zweifel, L. S., & Palmiter, R. D. (2013) Genetic identification of a neural circuit that suppresses appetite; Garfield, A. S., Li, C., Madara, J. C., Shah, B. P., Webber, E., Steger, J. S., ... & Lowell, B. B. (2015) A neural basis for melanocortin-4 receptor–regulated appetite)
Data exclusions	Mice in behavioural or tracing experiments were excluded from analysis if vector expression was absent, incomplete or outside the area of interest. Exclusion criteria were pre-established.
Replication	All behavioural experiments were performed with at least two cohorts of mice. All replications were successful.
Randomization	Littermates were randomly assigned to either control or experimental groups.
Blinding	The investigator was not blinded to experimental or control groups during behavioural experiments. However, all behavioural experiments involved stereotaxic injections thus blinding the investigator to whether the mice passed or failed viral expression exclusion criteria.

Reporting for specific materials, systems and methods

We require information from authors about some types of materials, experimental systems and methods used in many studies. Here, indicate whether each material, system or method listed is relevant to your study. If you are not sure if a list item applies to your research, read the appropriate section before selecting a response.

Materials & experimental systems

Methods

n/a	Involved in the study	n/a	Involved in the study
<input type="checkbox"/>	<input checked="" type="checkbox"/> Antibodies	<input checked="" type="checkbox"/>	<input type="checkbox"/> ChIP-seq
<input checked="" type="checkbox"/>	<input type="checkbox"/> Eukaryotic cell lines	<input checked="" type="checkbox"/>	<input type="checkbox"/> Flow cytometry
<input checked="" type="checkbox"/>	<input type="checkbox"/> Palaeontology	<input checked="" type="checkbox"/>	<input type="checkbox"/> MRI-based neuroimaging
<input type="checkbox"/>	<input checked="" type="checkbox"/> Animals and other organisms		
<input checked="" type="checkbox"/>	<input type="checkbox"/> Human research participants		
<input checked="" type="checkbox"/>	<input type="checkbox"/> Clinical data		

Antibodies

Antibodies used	Rabbit anti-CGRP (Bachem, T4032) Lot: A15513, 1:1000 dilution. Rabbit anti-serotonin (Immunostar, 20080), Lot: 1431001, 1:1000 dilution.
Validation	Both antibodies are listed on the JCN Antibody Database. Rabbit anti-CGRP (T4032) has been shown to lack staining when pre-adsorbed with CGRP when immunostaining mouse trigeminal ganglion (Kosaras et al., 2009, J Comp Neurology). Rabbit anti-serotonin (20080) has been shown to lack staining when pre-adsorbed with BSA-Serotonin when immunostaining mouse brain sections (Alonso et al., 2013, Brain Structure and Function)

Animals and other organisms

Policy information about [studies involving animals](#); [ARRIVE guidelines](#) recommended for reporting animal research

Laboratory animals	All mice were used were of C57BL6/J background. Surgery was conducted on male mice from at least 6 weeks of age. Behavioural experiments were then conducted at least 3 weeks after surgery. Electrophysiology was performed using both male and female mice from 3-6 weeks of age.
Wild animals	This study did not involve wild animals.
Field-collected samples	This study did not involve field-collected samples.

Ethics oversight

All procedures were conducted according to the Korean Advanced Institute of Science and Technology (KAIST) Guidelines for the Care and Use of Laboratory Animals and were approved by the Institutional Animal Care and Use Committee (Protocol No. KA2018-80).

Note that full information on the approval of the study protocol must also be provided in the manuscript.